DOI: 10.1002/anie.200703693

Touch Sensors

Tactile Devices To Sense Touch on a Par with a Human Finger

*Vivek Maheshwari and Ravi Saraf**

Keywords:
materials science · molecular electronics · nanostructures · sensors · thin films

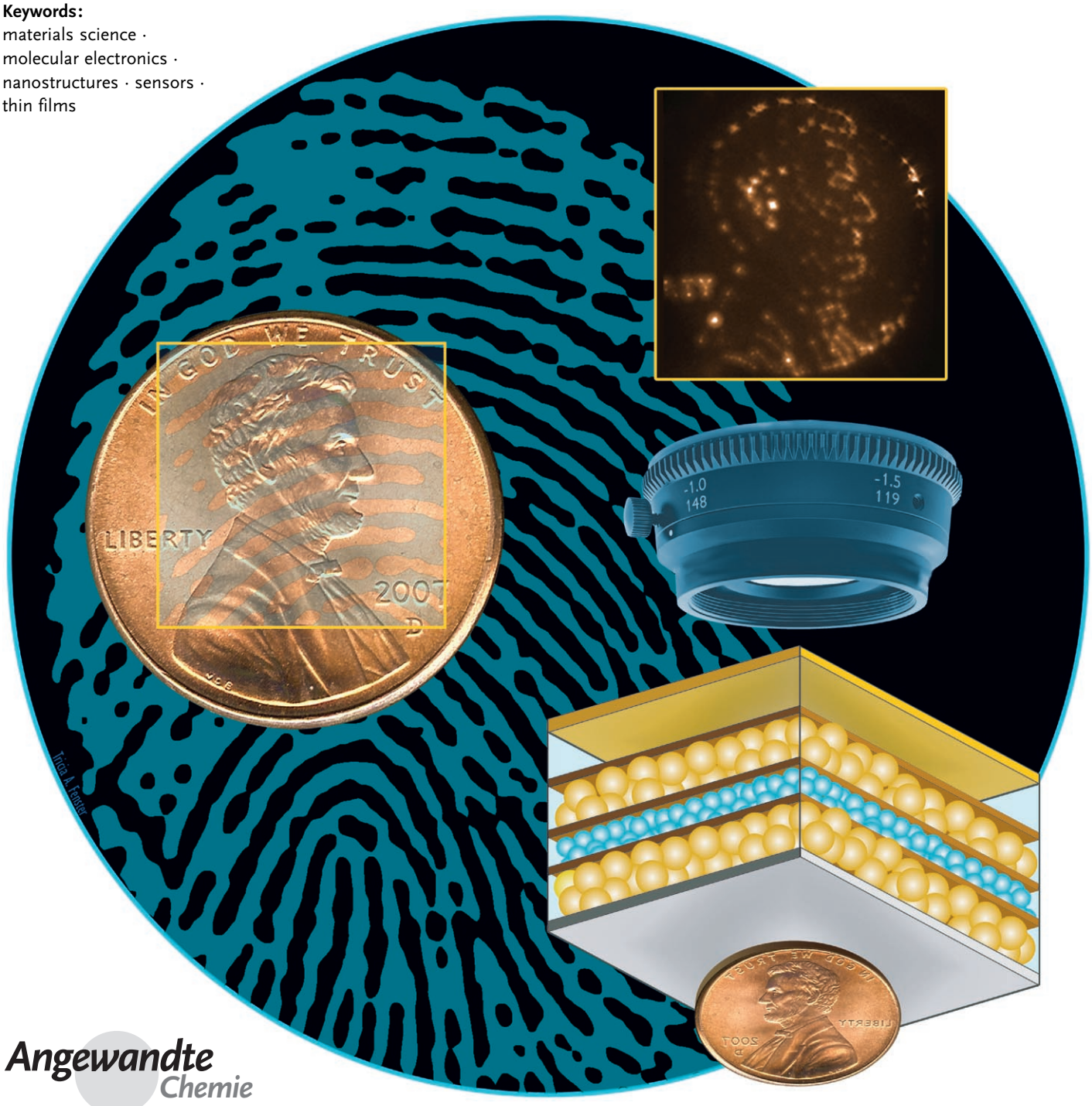

Our sense of touch enables us to recognize texture and shape and to grasp objects. The challenge in making an electronic skin which can emulate touch for applications such as a humanoid robot or minimally invasive and remote surgery is both in mimicking the (passive) mechanical properties of the dermis and the characteristics of the sensing mechanism, especially the intrinsic digital nature of neurons. Significant progress has been made towards developing an electronic skin by using a variety of materials and physical concepts, but the challenge of emulating the sense of touch remains. Recently, a nanodevice was developed that has achieved the resolution to decipher touch on a par with the human finger; this resolution is over an order of magnitude improvement on previous devices with a sensing area larger than 1 cm^2. With its robust mechanical properties, this new system represents an important step towards the realization of artificial touch.

From the Contents

1. Introduction

Sensor devices are critical to the development of tools that can enhance or replace human intervention. Sensors interface with the environment, similar to the five human senses of hearing, smell, touch, vision, and taste, to stimulate a suitable response or action. Among the first four senses, touch remains the most challenging sense to emulate, where capabilities on a par with a human finger are required. The difficulty lies in designing a high-resolution device that can be mounted on a curved surface and also sense a distribution of stimuli at high spatial resolution over a large area of contact. For example, a human finger—the most sensitive touch sensor known—can feel texture by detecting surface roughness at a spatial resolution of about 40 μm[1] over a contact-area of approximately 1 cm^2 and at stress levels of 10–40 KPa;[2] in contrast, current sensor devices have a resolution of 2 mm for a similar contact area.[3]

Despite their limitations, the importance of touch or tactile sensors is well recognized. The lack of the sensation of touch has been a common frustration for surgeons during minimally invasive surgery (MIS), where it becomes difficult to discern the pathology of tissue, for example, cancer versus healthy, or vascular versus connective tissue, by vision alone.[4–8] Touch is a critical sense that provides unique information to augment other senses in the perception of contact, motion, shape, and texture.[9] Although the human skin senses the distribution of pressure (or stress) over the area of contact to discern shapes and texture,[10] it also measures other stimuli, such as temperature and wetness. In this Review, we will focus only on the sensing of the pressure distribution over the area of contact. Furthermore, this discussion will be focused on the transduction aspect of the device for converting the local contact force into a measurable signal. As the typical contact area by a human finger is about 1 cm^2, we will further limit our discussion to tactile sensing devices with a comparable area of contact. Special emphasis is given to new possibilities emerging from current research on nanomaterials and nanodevices. We will not discuss single-point sensors,[11] which determine the occurrence of contact, or one-dimensional row-of-point sensors, which measure the dynamic pressure for determination of motion or slip relative to the sensor surface.[12]

Robotics and minimally invasive surgery are among the primary driving forces for the development of devices that emulate the sense of touch (also referred to as electronic skin). In robotics, the emphasis is on building humanlike robots (humanoids) that can perform in an unstructured environment, such as in a house or in rescue operations. Humanoids capable of performing household chores are considered the next revolution after personal computers.[13] However, without a high-resolution touch sensation on the hands of the humanoids, simple tasks, such as pouring and serving a glass of water or folding laundry, become very complex and lengthy.[14–19] Theoretical models have been developed to optimize the contact configuration for holding objects as well as the dynamics of grasping;[20] however, a significant barrier to developing a practical system is the lack of high-resolution and large-area touch sensation, which makes optimizing a difficult task. MIS is one of the fastest growing developments in medicine which improves the patients post-surgery prognosis and reduces hospital costs. It could potentially enable surgeons to provide care in remote areas by remote control or by robotic surgery, with the physical presence of the surgeon not required.[21] While significant progress has been made over the last three decades in these areas, the lack of high-performance tactile sensors has been recognized as one of the critical bottlenecks.[22] For example, today a surgeon operating by MIS is primarily dependent on his/her vision, thus making it difficult to decipher cancerous tissue from normal tissue, because it is not possible to "feel" the texture[5] or distinguish between

[*] Dr. V. Maheshwari, Prof. R. Saraf
Department of Biomolecular and Chemical Engineering
University of Nebraska, Lincoln
207 Othmer Hall, Lincoln NE 68588-0643 (USA)
Fax: (+1) 402-472-6989
E-mail: rsaraf@unlnotes.unl.edu

stones and air bubbles during a laparoscopy.[7] Thus, if tools, ranging from a simple catheter to a microrobot could be covered with an electronic skin, the sophistication of MIS and its potential applications could be greatly improved, thereby reducing patient recovery time and cost.

The underlining premise or hypothesis of this Review is that if it is possible to develop a tactile sensor with a form similar to skin and a performance close to a human finger, it will produce high quality data (input) which will significantly enhance MIS and robotics for operations such as in vivo assessment of tissue pathology and those requiring grasping.[1] Furthermore, analogous to human memory, high quality tactile information can be stored to "teach" the robot to learn to work in an unstructured environment such as a home.

This Review is not a critical comparison of the various devices/ideas, but rather an effort to stress the multidisciplinary nature of the problem in the hope of generating new ideas among the readers. The development of an electronic skin will require high-performance tactile sensors that mimic human skin in terms of touch sensation over a large area (over 1 cm^2), high flexibility, resolution, and sensitivity comparable to a human finger, as well as ease of signal extraction for speed and implementation.

We begin with an overview of the human skin (Section 2), which is the inspiration and benchmark in developing a robotic hand and designing tools for MIS. We are interested foremost in the tactile (device) aspect of the human skin, thus we will emphasize the device characteristics rather than discuss the physiology of the neural sensors. There are several excellent descriptions in the literature of the neural physiology to sense touch.[23–26] Two aspects of the skin are highlighted in Section 2: the natural sensor is intrinsically digital and the viscoelastic ability of the skin to transmit mechanical strain enhances the sensitivity for dynamic sensing. We illustrate the connection between the viscoelastic nature of skin and dynamic sensing, an area that is not well studied or represented in the literature and which today remains one of the key limitations in sensors.[14]

Two possible approaches to designing a tactile-sensitive transducer have emerged: 1) building a micrometer-scale structure that produces a well-behaved response when perturbed by strain arising from physical contact, or 2) tailoring the chemistry at the molecular level to design a material that intrinsically converts strain (on touch) into a signal (usually electrical or optical). In Section 3, we briefly outline the most common current designs for each of the two approaches. Each of the subsections concludes with (speculative) ideas based on recent research and developments in molecular electronics, one-dimensional nanomaterials, such as nanowires and nanotubes, and self-assembled nanostructures that may have the potential for making higher resolution devices based on the (current) microscopic structures. In Section 4 (based primarily on our work) we describe a device made by the self-assembly of nanoparticles. Although the device is based on the highly nonlinear (quantum mechanical) principle of electron tunneling, the response is linear, as shown experimentally and modeled theoretically. The spatial resolution for touch perception and sensitivity of the device is on a par with a human finger. In principle, because the fabrication consists of simple sequential dip coating, the device can be made on large surfaces of high curvature, a feature none of the current tactile devices can duplicate to our knowledge. In Section 5 we highlight the current challenges that need to be met to emulate human skin in terms of both performance and physical form.

2. The Natural Tactile Device: The Skin

The skin is the largest organ in the human body. It covers the entire body and provides a variable degree of sensitivity to perceive touch. Fingertips, the most sensitive tactile sensor, have the shape and agility to sense texture and hardness, as well as to grasp objects based on the sensation of touch. The goal of this section is to describe this most sophisticated of tactile sensors in terms of overall performance, which will serve both as a benchmark and the inspiration for new ideas. As a tactile device, skin can be considered a hybrid system composed of the active sensor—the neuron—imbedded in a viscoelastic media—the dermis—which transmits strain from the mechanical contact to the neuron. The dermis serves as a packaging material to hold the network of neurons, and plays a critical role in achieving dynamic sensing. Therefore, to build a successful tactile device, it is critical to analyze the problem at a "system" level rather than just consider the performance of the sensor alone. In Section 2.1 we discuss the mechanical properties of the dermis followed by the characteristics of the imbedded neurons.

Vivek Maheshwari completed his BS at the Indian Institute of Technology, Delhi, and his MS at Wayne State University, Detroit, both in Chemical Engineering. In 2006 he completed his PhD in the "Macromolecular Science and Engineering program" at Virginia Tech. Since 2007 he has been a research assistant professor with the "meso scale" research group at the Biomolecular and Chemical engineering department of University of Nebraska, Lincoln. His research is in the area of devices based on nanomaterials, nano-biotechnology, and polymers.

Ravi F. Saraf is the Lowell E & Betty Anderson Professor of Biomolecular and Chemical Engineering at the University of Nebraska, Lincoln. He received his BS from the Indian Institute of Technology, Kanpur, in 1980 and an MS and PhD from the University of Massachusetts, Amherst, in 1987, all in chemical engineering. He spent five years as a faculty with the Chemical Engineering department of Virginia Tech and ten years at the IBM T. J. Watson research centre. His research interests include nanotechnology, material science, applications of nanomaterials in devices, biosensors, and polymers.

2.1. Viscoelastic Properties of the Dermis

Human skin consists of an outer epidermis layer which is 0.06 to 0.12 mm thick. It simply protects the 1 to 4 mm thick dermis layer containing the tactile sensors.[27,28] When skin is subjected to external stress upon touch, the strain is transmitted through the dermis to the neurons, which send a signal to the brain.[10,23,28] Since the response is to the local deformation[10] of the skin, the sensitivity and performance of the sensors intrinsically depends on the mechanical properties of the dermis.[29–32]

The dermis is viscoelastic in nature, which causes the mechanical (strain) signal transmitted to the imbedded neurons to be sensitive to both the magnitude of the external stress (local) and its rate of change on touch.[33] The primary component that imparts the viscoelastic nature to the dermis is the extracellular matrix (ECM), which is composed of a network of elastic and collagen fibrils.[34,35] Collagen constitutes between 66–69 % of the volume fraction in dermis.[31,34] The modulus of collagen fibers is pH-dependent as the charge of their constituent carboxylic and amine groups varies with the pH value.[36,37] The elastic fibers are composed of elastin and microfibrillar-associated glycoprotein. The fibers vary in diameter from 1 to 2 μm in different layers of the dermis and contain varying amounts of elastin. The elastin regions also exhibit different levels of ordering, depending on their location in the dermis. The relative amount of elastic fibers increases in the dermis from 1.7 % in the upper layer to 2.5 % in the lower layer.[28,38] Thus, the mechanical property of the dermis is non-uniform as a function of depth. The viscoelastic nature of the ECM arises from a combination of the elasticity from the stretching of the elastic and collagen fibril networks, and the viscosity is due to the interfibril slippage at the network junctions.[25,38–41]

The viscoelastic behavior of skin is illustrated by applying stress-relaxation cycles (Figure 1).[28] The stress is monitored continuously as the skin is strained incrementally in steps. Each step increase in strain is followed by a holding time where the strain is held constant and the relaxation in stress from the instantaneous maximum values is noted until equilibrium is reached (Figure 1 a). The final equilibrium stress is the elastic component, as it is the stored elastic energy, and the dissipated stress (the difference between the maximum and equilibrium value) is the viscous component (Figure 1 b). This behavior is analogous to a highly entangled, high-molecular-weight polymer melt, where polymer chains form a network because of entanglements. The stretching of the chains between the entanglement junctions makes the melt elastic while the slippage between the chains at the entanglement junctions causes a viscous dissipation during deformation.[33]

Although the viscoelastic nature of the dermis is reported in the literature, its link with the ability of skin to conserve energy and sense dynamic strain caused by, for example, moving a finger over a surface is not appreciated. We illustrate this concept by considering the dermis to be a simple, viscoelastic material that can be modeled as a linear superposition of viscous liquid and elastic solid (Figure 2 a).[33] The viscous component is a dashpot that emulates a liquid of viscosity η, and the elastic nature is represented by a (perfect) spring of modulus E_1 and E_2. In response to an arbitrary compressive strain $\varepsilon(t)$ (caused by external stress on touch), the reactive stress generated in the two parallel elements is $\sigma_1(t)$ and $\sigma_2(t)$. As the pure elastic and viscoelastic elements in the model are in parallel, the total strain in the two elements is the same. The total stress $\sigma_1 + \sigma_2 = \sigma$ felt by the neuron can be calculated by solving Equation (1).

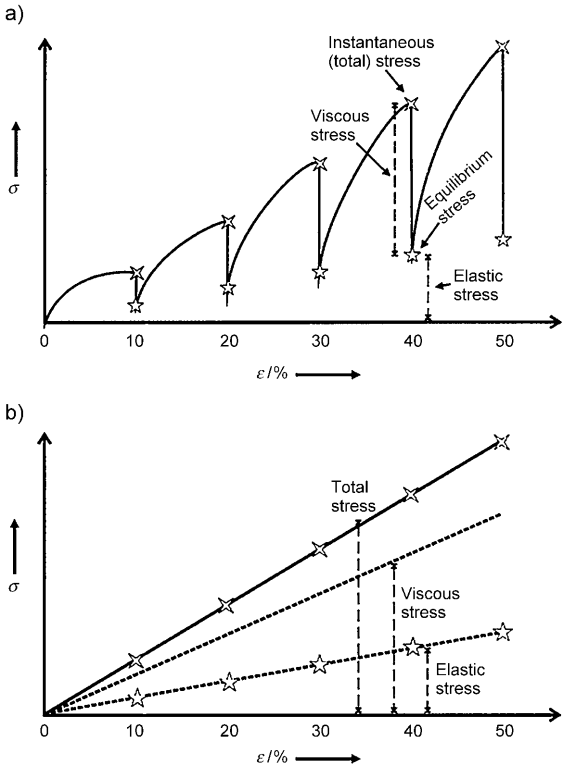

Figure 1. The viscoelastic response of skin to stress/relaxation cycles; ε: stress, σ: relaxation. a) Incremental straining of the skin with a holding period shows the stress relaxation from instantaneous maximum values to the final elastic stress.[28] b) Total stress and elastic and viscous stress components from the stress relaxation cycles of (a).[28] Reprinted with permission from Ref. [28]. Copyright Blackwell Munksgaard.

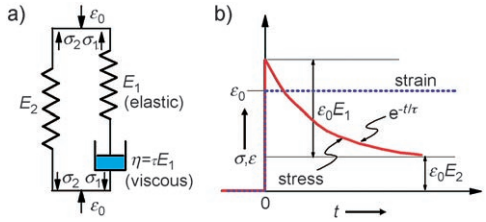

Figure 2. Viscoelastic response from a model element consisting of pure elastic and viscous elements. a) A parallel combination of a spring (elastic element) and a dashpot (viscous element) in series with a spring is used to simulate the viscoelastic response of skin. b) Viscoelastic response to a step strain (ε_0) applied to the model element. The stress relaxes from maximum values (because of the viscous nature) to a constant level determined by the elastic element (E_2) at a rate determined by the viscous element (η/E_1).

$$\frac{d\varepsilon}{dt}=\frac{1}{E_1}\frac{d\sigma_1}{dt}+\frac{\sigma_1}{\tau E_1}=\frac{1}{E_2}\frac{d\sigma_2}{dt} \quad (1)$$

Figure 2b shows the stress generated when a surface is suddenly brought into contact with skin (simulated by the viscoelastic model of Figure 2a) to strain the skin (in compression) by ε_0 at time $t=0$. The total stress σ increases suddenly to $\varepsilon_0(E_1+E_2)$, because of the elastic nature of the model. However, unlike elastic material, the stress relaxes exponentially to $\varepsilon_0 E_2$ because of the viscous nature of the material (emulated by the dashpot). The relaxation time τ of the exponential decay is η/E_1. In other words, the skin will send a signal on contact that will ultimately subside to a lower constant value. Thus, the viscoelasticity allows a high signal to register the contact, but the stress generated in response to the contact gradually lowers by the factor $|E_2|/(E_2+E_1)$ (similar to the observation in Figure 1). As a result, even though the contact is maintained, the firing of neurons is reduced due to stress relaxation, thereby conserving energy.

Dynamic sensing as a result of the viscoelastic nature of the dermis is illustrated by quantifying the stress produced in the dermis by periodic external stimuli, for example, when a finger is caressed at a constant (initial) force over a periodic textured surface. Figure 3a idealizes a textured surface as a periodic square wave. Ignoring the distribution of stress over the contact area because of the texture, the (average) strain $\varepsilon(t)$ will modulate over some constant strain ε_c. The constant strain ε_c is proportional to the constant initial force applied by the finger on the surface to gauge the texture. For a texture not too deeply etched, the strain arising from texture is a periodic modulation of amplitude ε_0, which is above ε_c, and $\varepsilon_c \gg \varepsilon_0$ (Figure 3b). The time period of the strain modulation T is inversely proportional to the scanning speed of the finger. By solving Equation (1) with the Laplace transform, the resulting stress arising from the input strain from the texture, that is, $\varepsilon(t)$, is given by a periodic function where the first period for $0 \le t \le T$ is given by Equation 2 (Figure 3c), where, $u_{aT}(t)$ is a unit step function with a step at $t=aT$. As the human body is composed of a significant amount of fluids (such as blood), the relaxation time is reasonably short compared to T, that is, $T/\tau \gg 1$. Figure 3c shows the total stress response.

$$\sigma(t)=\sigma_1(t)+\sigma_2(t)=\varepsilon_0 E_1[e^{-t/\tau}-e^{-(t-T)/\tau}u_{aT}(t)]+\varepsilon_0 E_2 \quad (2)$$

Two related features in Figure 3c,d demonstrate the enhancement effect arising from the viscoelastic nature of the finger: 1) If the ECM was completely elastic, the stress response would be similar to $\sigma_2(t)$, with an amplitude of $E_2\varepsilon_0$ instead of $(E_1+E_2)\varepsilon_0$ (Figure 3c). The fast relaxation results in the edges being enhanced as "stress spikes". 2) Furthermore, from Equation (2), the relaxation enhances the contrast between the two edges of the square function (Figure 3c) from $\Delta=(E_1+E_2)\varepsilon_0$ for pure elastic ECM to $\Delta=(2E_1+E_2)\varepsilon_0-E_1\varepsilon_0 e^{-aT/\tau}\approx(2E_1+E_2)\varepsilon_0$ for viscoelastic ECM with fast relaxation, namely, $T/\tau \gg 1$. For typical modulii of the dermis, the enhancement $E_1/(E_1+E_2)$ is 40–50 %.[28] The faster the relaxation and slower the scan rate, the better is the enhancement in the contrast. As will be discussed in Section 2.2, the skin has specialized sensors (Pacinian corpuscles) that do not have good spatial resolution but respond to high speed vibration and will sense the periodic spikes to discern the texture. As a person ages, skin loses its elasticity (E_1 and E_2), thereby reducing both the elastic response $E_2\varepsilon_0$ and the contrast $E_1\varepsilon_0$ arising from the viscoelastic behavior.[35,42]

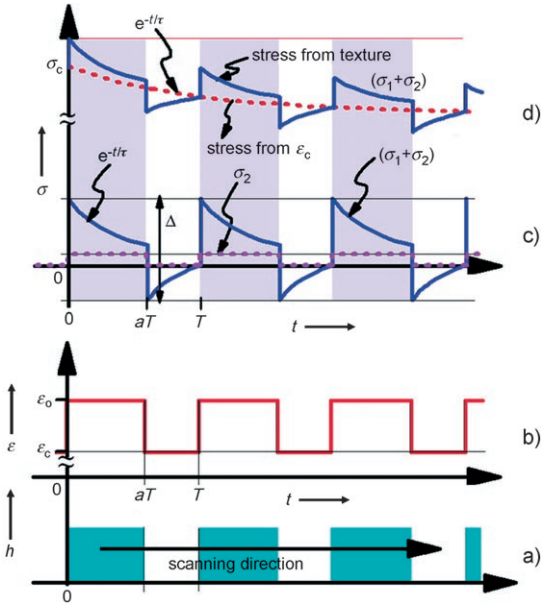

Figure 3. Stress response of the model viscoelastic element in Figure 2a from a periodic strain stimulus generated by, for example, scanning the finger across a periodic textured surface. a) Cross-section of a periodic textured surface made of lines of equal width. b) On rubbing a finger on the textured surface at a constant velocity, the base strain of ε_c, arising from the constant average pressure applied by the finger, will modulate as a square wave in strain with a peak strain of ε_0. c) The stress response from the periodic modulation alone shows a typical viscoelastic behavior with sharp stress maxima at the rising and falling edges of the square strain modulation. The viscoelastic behavior (stress relaxation) results in the strain being negative at the falling edges, which corresponds to extension, and the stress maxima at the edges are more conspicuous than for a pure elastic material. d) The total stress response showing the added relaxation of the stress as a consequence of the constant strain ε_c.

2.2. Digital Behavior and Specialization of Neurons

The stress generated in the dermis in response to external stimuli on touch is sensed by touch receptors, namely, neurons (Figure 4),[24–26] which send a signal, in the form of electrical pulses, to the brain. The inner (resting) potential of the neuron at no stimulus is approximately −70 mV relative to the surrounding dermis. The inner region of the neuron has excess K^+ ions, and the extracellular dermis region is rich in Na^+ ions. In response to a stimuli, the Na channels of the neural membrane open, causing Na^+ ions to diffuse in the neuron, thereby leading to an increase in potential (relative to the dermis) to about +30 V; at this point the K channel is triggered to let the K^+ ions diffuse, which causes the potential to drop to about −90 mV. Thus, a pulse of about 100 mV

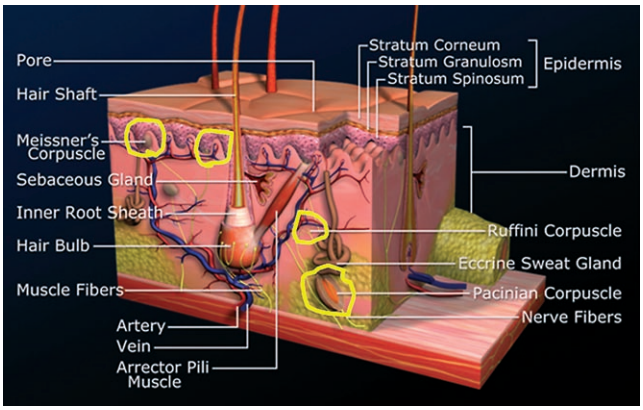

Figure 4. Schematic representation of the skin showing the receptors (marked in yellow) for sensing touch as well as the epidermis and dermis layers. Receptor classification: Near field: Merkel corpuscle (SA I, the receptor without a label in the figure), Meissner corpuscle (FA I). Far field: Ruffini corpuscle (SA II) Pacinian corpuscle (FA II). Figure reprinted with permission from 3Dscience.com.

relative to the resting potential is generated and transmitted to the brain. The system (relatively slowly) relaxes back to −70 mV by active transport of the ions.[43] The frequency of the pulses created is proportional to the magnitude and rate of the stimuli.[44–48] Figure 5 shows the measured rate of pulses

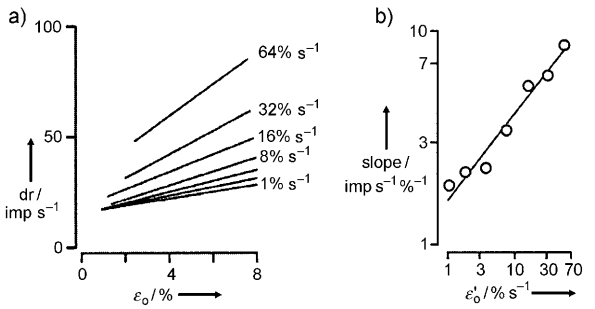

Figure 5. The discharge rate measured as the impulse rate discharged from the nerve (impulse per second, imp s^{-1}) for SA receptors increases linearly with strain amplitude ε_0 and strain rate ε'_0. a) The SA III receptors show a linear increase in discharge rate with strain amplitude.[46] b) The discharge rate increases linearly with the strain rate, measured as the strain velocity for SA I unit.[46] Reprinted with permission from Ref. [46]. Copyright American Physiological Society.

for a typical receptor as a function of strain at various strain rates.[46] The digital response, that is, frequency of pulses, is linear with respect to the strain magnitude. Furthermore, Figure 5b shows that the change in the slope of the line in Figure 5a increases linearly with the strain rate.[46] Hence, the response to the stimuli is intrinsically digital and linear. Nerve activity or pulse generation from touch receptors is observed when strains as low as 0.5 % are applied to the epidermis.[46,49]

The second interesting aspect of the natural tactile device is the variety of sensors in terms of response speed and the relative depth of the active sites of the sensors from the skin surface. The dermis has two primary classes of touch receptors: the slow acting (SA) ones, which respond to sustained strains, and the fast acting (FA) ones, which respond to strain rates.[45,49,50] For example, FA receptors can send neural pulses at frequencies as high as 1000 pulses per second as the strain rates change rapidly during the initiation of touch, while SA receptors can respond at frequencies as low as 2 pulses in 5 seconds, which conserves energy on prolonged touch (Table 1).

Table 1: Response characteristics of the four primary receptors, SA I, FA I, SA II, and FA II.

Type of receptor	Response characteristics
Merkel (SA I) (near field with multiple sensitive points; continuous, irregular discharge)	slow, fine details, 0.4–100 Hz
Meissner (FA I) (near field; ON-OFF discharge)	slightly faster, grip control, 10–200 Hz
Ruffini (SA II) (far field; continuous, regular discharge)	slow speed, stretching, 0.4–100 Hz
Pacinian (FA II) (far field; ON-OFF discharge)	fast, vibration, dynamic texture, 70–1000 Hz

The FA and SA receptors are further differentiated on the basis of their receptive fields. The FA I and SA I receptors are closer to the skin surface and respond to highly local external stress (Table 1, Figure 4) and are, therefore, called "near-field" receptors. The "far-field" receptors SA II and FA II are imbedded deeper in the dermis and have broad receptor fields of touch sensitivity.[46,50] Receptors with broad receptor fields can respond to "remote strains," namely, strains far from their physical locations. For example, a highly localized strain, generated by a sharp pinpoint, will even be detected by remote, large receptor field sensors but only by near-field sensors in the vicinity.

Another important feature in regard to the human finger as a tactile device is the distribution of the sensors in the hand.[51] The near-field devices are located close to the surface of the skin and have well-defined receptive fields; hence they are linked to sensing texture and are present in high density at fingertips. The far-field receptors, which are more evenly distributed over the palm and fingertips and have large receptive fields, are thought to play a role in perceiving the motion of joints and maintaining grip while also providing a sensation when objects slip.[44–46,49,50,52–54] Tactile information is also deciphered from the latency of receptors in firing the first impulse to a tactile stimulation, thus relating the threshold of receptors in sensing touch to a tactile neural signal.[55]

The presence of two polymer networks in the skin, one with low modulus (elastic fibers) and one with higher modulus (collagen fibers) results in both the compliance of the skin in

deforming to the surface features and their detection at high strains. The viscoelastic character is also important for absorbing the energy during viscous deformation because of surface features and providing a reversible mechanical deformation to detect the features. Artificial systems have not emulated two aspects of the active components of the natural tactile device: 1) the sensing system is completely digital, making the system prone to less error, a low noise level, and high sensitivity. The intensity of the signal is registered as the number and frequency of pulses generated by the neural activity, and 2) the variety of receptors and their characteristics of neural activity result in an intricate signal-generation pattern to applied strain and strain-rate distribution. Both the static and dynamic distribution of the strain on the area of contact is measured with (nominally) an independent set of sensor devices.

3. Tactile Devices: Current State and Outlook

Generically, tactile devices are composed of a tactile-sensitive element that produces a signal in response to a mechanical contact and a data-acquisition system that collects the signals for analysis. Two strategies have emerged for the development of the tactile-sensitive element: 1) development of a structural unit that generates a signal on touch (Section 3.1) or 2) the use of materials that, at the molecular level, intrinsically convert the mechanical strain on touch into an optical or electrical signal (Section 3.2). Although the emphasis of the Review is on a tactile-sensitive element, it is critical to consider the complete system of signal generation and extraction to make a (potentially) successful tactile device.

3.1. Tactile Devices Based on Micro- and Nanoscale Structures

Tactile sensors in which a structure is designed to produce a signal in response to the local strain are termed "active structure" tactile sensors. Section 3.1 is divided into three parts. In the first two, we discuss two common configurations of the active structure used for making tactile devices, and in the third section we speculate on potential high-performance devices based on recent research (especially in nanomaterials).

3.1.1. Tactile Devices with an Array of Capacitors

A capacitance-based tactile device consists of an array of capacitor cells where each cell or pixel consists of two identical parallel metal plates or electrodes of area A separated by a distance D with a flexible spacer of relative dielectric constant ε_r (Figure 6). The capacitance of this parallel-plate capacitor is given by Equation (3), where ε_0 is the (electric) permittivity of a vacuum and C_f is the contribution from edges of the electrode (which would tend to store more charge than the rest of the electrode). Typically, $A \gg D^2$ in all designs for tactile sensors, therefore, the C_f term is negligible.[56]

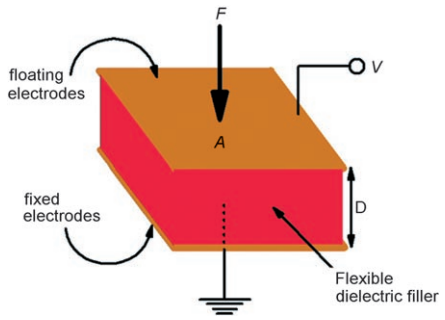

Figure 6. A parallel plate capacitor consisting of two parallel plates of area A separated by a flexible insulator of relative dielectric constant ε_r. The thickness of the dielectric film is D. F: force, V: bias.

$$C = 4\pi\varepsilon_r\varepsilon_0\frac{A}{D} + C_f \quad (3)$$

In a typical tactile device an array of such capacitor elements (or pixels) are fabricated by using micro-electro-mechanical systems[57–60] (MEMS) technology.[61,62] The top electrode, where the contact pressure is applied, is deposited on a flexible filler (Figure 7a) and, therefore, it is mobile in

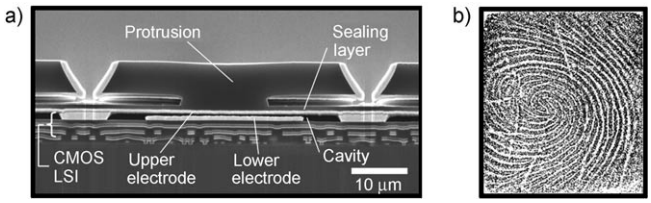

Figure 7. a) A cross-sectional schematic representation of a capacitor element made by MEMS technology. The protrusion is the pixel where F was applied, which pushes the upper electrode toward the lower electrode.[65] CMOS: complementary metal oxide semiconductor, LSI: large-scale integrated circuits. b) The change in capacitance between the electrodes is measured on each pixel and mapped to form an image, for example, a human fingerprint.[65] Reprinted with permission from Ref. [65]. Copyright IEEE.

the verical direction with respect to the fixed, bottom electrode.[63–66] The contact pressure causes a change in thickness $\Delta D = FD/AE$, where F is the applied compressive force on the pixel, namely, the top electrode surface, and E is the compressive modulus of the flexible filler. For a non-ferroelectric material, ε_r is independent of stress. As $D^2 \ll A$, A is nominally constant on deformation. Thus, from Equation (3), the change in capacitance ΔC is given by Equation (4), where G is the bulk modulus.[67]

$$\Delta C = C\frac{F}{AG} = \frac{4\pi\varepsilon_r\varepsilon_0}{GD}F \quad (4)$$

Figure 8 shows a linear relationship between the relative change in capacitance $\Delta C/C$ and the load (stress, σ, F/A), which is consistent with Equation (4).[67] Furthermore, from Equation (4), the sensitivity of the device increases when the filler is more compliant (E is low), the separation between the

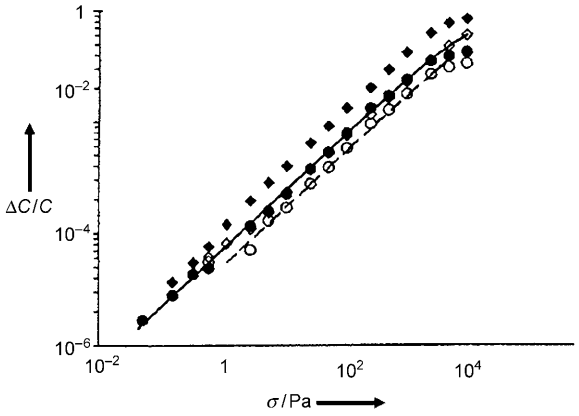

Figure 8. Comparisons of the relative change in capacitance ΔC with load σ for air-filled and polymer-filled capacitors; Dow 2103: air ◇, polymer ◆; polyester: air ○, polymer ●. A linear relationship consistent with Equation (4) is observed.[67] Reprinted with permission from Ref. [67]. Copyright IEEE.

electrode is as small as possible (D is small), and the dielectric constant is as high as possible (ε_r is large). For most polymers that are ideal fillers because of a low E value, ε_r is small—typically less than four. Therefore, ferroelectric polymers that have large ε_r values (ca. 15–20) are the ideal choice, as will be discussed in Section 3.2.

For a typical capacitor element without a sophisticated on-chip signal-conditioning circuit, the limit of capacitance for achieving a feasible signal-to-noise ratio is on the order of 1 pF.[67] This limit translates to an area of 0.1 mm^2 for a separation distance of 1 μm between the capacitor plates or a square capacitive element with a size of about 350 μm. However, capacitor elements, that is, pixels, as small as 50 μm squares have been fabricated with an on-chip signal-conditioning circuit to observe fine texture, such as a fingerprint (Figure 7b).[65]

3.1.2. *Flexible Tactile Devices with Conductive Polymer Composites*

The use of conductive polymer composite films in the generation of tactile sensors is perhaps the most successful transduction principle for building large-area devices spanning over tens of cm^2. Such films are used in a variety of configurations to make some of the simplest and the most sophisticated tactile sensors. Sensors based on conductive composites is, to our knowledge, the only approach (other than the recently reported device discussed in Section 4) that can be used to make flexible tactile devices that can be wrapped around curved surfaces.[3]

A composite consisting of conductive filler particles in an insulating polymer matrix becomes conductive when the volume fraction of the particles is above a certain value, the percolation threshold. The threshold is defined as the volume fraction of the conducting particles where there is at least one channel spanning the sample to form a conducting (percolating) pathway. Theoretically, the percolation threshold for uniformly dispersed particles, that is, random distribution, is about 16% by volume.[68,69] In practice, even if the dispersion of the conducting filler is close to uniform in the matrix, the system is not "mathematically" random, thereby resulting in a threshold that may be well below 1% to above 30%. The primary reason for such a wide range in the percolation threshold is the shape of the filler, which affects its spatial distribution. For example, if the filler is fiberlike with a large radius of gyration, the threshold can be over two orders of magnitude lower than for spherical particles. Therefore, high aspect ratio fillers, such as conductive surfactants and carbon nanotubes, result in composites that are conducting even with a volume fraction of fillers below 1%.[68,70,71] In contrast, the threshold is above 16% with Ag flakes and carbon-black particles, which tend to cluster into more dense structures.[68]

When this type of composite film is compressed, the polymer matrix deforms, thereby bringing the particles closer. This effect increases the number of percolating channels, which causes an increase in conductivity. If the relationship between the compressive strain, conductivity, and the mechanical properties of the composite film is known, the local strain (and stress) can be obtained by measuring the local conductivity through the film.[72,73] Figure 9 shows a

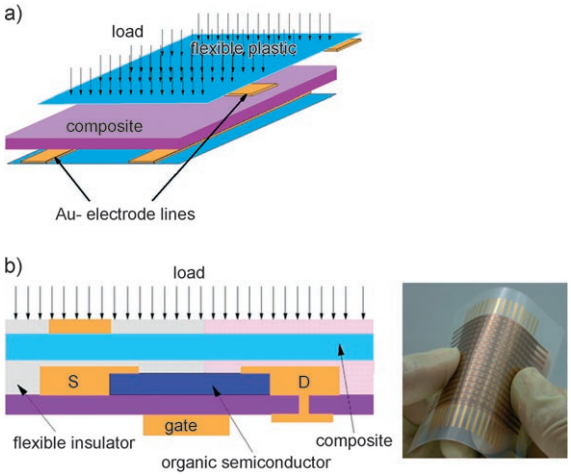

Figure 9. Active and passive device configuration. a) A passive device where an orthogonal electrode assembly is used to sandwich a composite filler film. b) An active device where the film is coupled with the source electrode of an organic transistor; S: source electrode, D: drain electrode. The inset is an image of a flexible tactile sensor made from an organic semiconductor.[3] Reprinted with permission from Ref. [3]. Copyright National Academy of Science, USA.

passive and an active configuration used to measure the modulation in the local resistance resulting from strain caused by stress distribution on contact. In the passive design, the composite film is sandwiched between an orthogonal set of electrode lines (Figure 9a). As the device is compressed, the electrodes come closer and the increase in current (at some fixed bias) is recorded to determine the local stress on the pixel (defined as the "intersection" of the two lines). As the applied external bias is scanned over the individual top and bottom electrode line, the current density over each intersection is registered to obtain the tactile image. The dynamic range of a passive device is limited, because of nonlinear and hysteresis effects, which mean that large deformations are not

possible. When the loading is increased to 60 KPa in passive devices, resistance declines by a factor of 30; however, the spatial resolution is limited to 5 mm.[73]

In the active configuration the composite film is coupled to a transistor (Figure 9b). In these devices, the current can increase over threefold for a threefold increase in the stress and can be controlled by the gate voltage (Figure 10a).[3] In a typical design, where each pixel is an organic thin film transistor, the devices are fabricated such that the flexible composite is in series with the source-drain electrode (Figure 10a). For a fixed gating voltage (V_{GS}), the resistance decreases as the composite is compressed, thus leading to an increase in the source-drain current (I_{DS}). Highly flexible tactile sensors, which can be wrapped around cylindrical surfaces, have been demonstrated with this design (see the inset in Figure 9b).[3] The salient advantage of the active device is its higher sensitivity and significantly lower power consumption compared to the passive device.

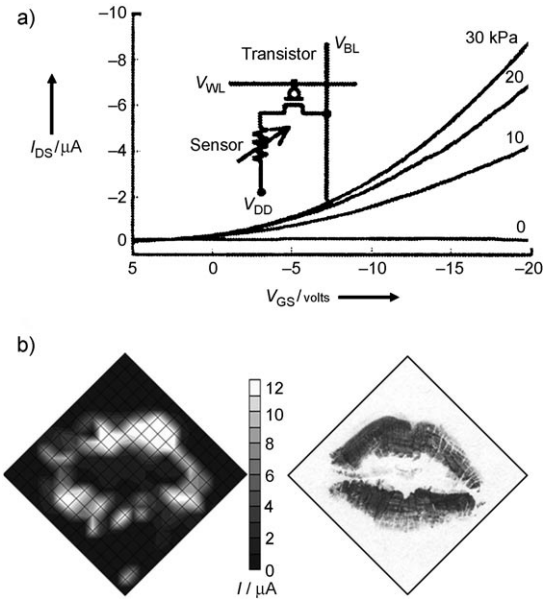

Figure 10. a) The drain current I_{DS}, the measured response of an active device, increases with stress. The sensitivity can be modulated by the gate voltage V_{GS} (the sensor control).[3] V_{BL}: bit line voltage, V_{WL}: supply line voltage, V_{DD}: supply voltage. b) Left: the image generated by the active tactile sensor (of (a)) on touching with a rubber replica of lips; the picture is constructed by mapping the current I in each pixel. Right: Imprint from the rubber lips on paper.[3] Reprinted with permission from Ref. [3]. Copyright National Academy of Science, USA.

Although the resolution for the device is approximately 1 mm (Figure 10b),[3] which is the highest for tactile devices with an active area above 1 cm^2 (except for the device described in Section 4), it is intrinsically limited because the conductivity of the composite is nominally isotropic. The resolution will significantly improve if the in-plane conductivity $\zeta_{\perp}$ is significantly smaller than the conductivity along the orthogonal direction $\zeta_{\parallel}$. Although no systematic studies have been performed to maximize the ratio $X = \zeta_{\parallel}/\zeta_{\perp}$, the shape of the particles should play an important role in optimizing X. A strategy to maximize X (a subject of future research) may be as follows: For an ideal random system, the percolation threshold in two and three dimensions is approximately 16% and 45% by volume.[69,74] Thus, the goal should be to make an "anisotropic composite" where the particles form a percolating channel in the direction orthogonal to the plane, but are well below the 2D threshold in the in-plane direction. A possible solution, discussed in Section 4, is to make a "structured composite" where the fillers (any shape) are deposited layer-by-layer such that X is very large.

3.1.3. More Sensitive, High-Resolution Tactile Devices Based on Nanostructured Materials

The use of conductive films for transduction (Section 3.1.2) has immense potential for making highly flexible films with high sensitivity. However, the current technology has two challenges: the dynamic range is small, that is, the composite responds to a limited range of strain, and the resolution is poor, because the composite has conductivity in the in-plane direction ($X = \zeta_{\parallel}/\zeta_{\perp}$ is large). The nanocomposite system in Figure 11a with aligned carbon nanotubes (CNTs)

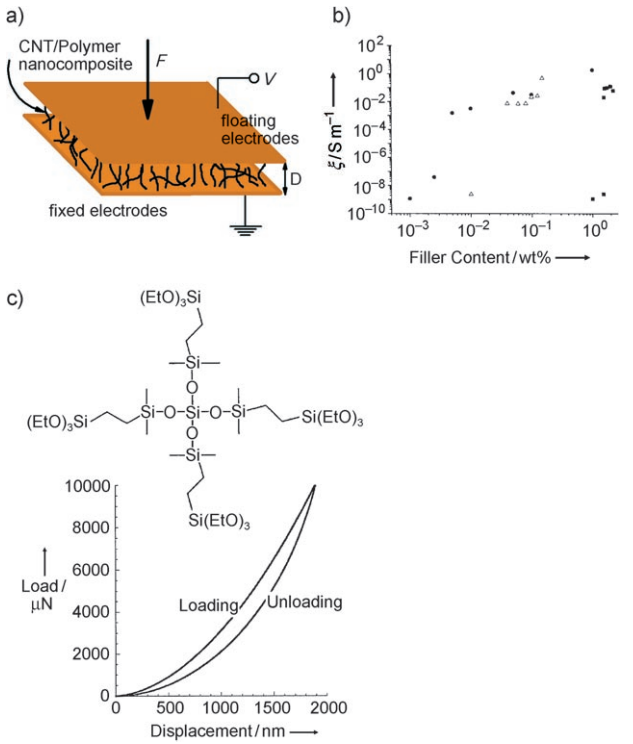

Figure 11. a) Schematic representation of a tactile pixel made using a composite of aligned CNTs and a gel matrix. b) The percolation threshold of the composite made with carbon black and CNTs as a filler in an epoxy matrix; ■ carbon black, △ entangled CNTs, ● aligned CNTs. The threshold, as measured by a rise in the specific conductivity, ξ (seimens per meter, $S\,m^{-1}$) as a function of filler content, is at least three orders of magnitude lower for aligned CNTs than carbon black.[68] c) The loading characteristic of a gel made from tetraalkoxysilane and star silane shows low hysteresis and large displacement. The inset shows the molecular structure of the star silane.[77] Figure 11b reprinted with permission from Ref. [68]. Copyright Elsevier Ltd. Figure 11c reprinted with permission from Ref. [77]. Copyright The Royal Society of Chemistry.

should meet both the challenges. The CNTs were dispersed in a gel by tethering the CNTs to an appropriate surfactant[75,76] to improve compatibility.

The resulting composite will have the following characteristics which are different from the currently used materials based on carbon-black particles in elastomers: 1) The percolation threshold with aligned CNTs is significantly small; more importantly, however, the rise in conductivity is significantly slower with a filler fraction just above the percolation threshold. This finding implies that there will be a large range of strain where the conductivity will rise monotonically before saturation (Figure 11b).[68] 2) As the percolation threshold with aligned CNT composites is three orders of magnitude lower than with the conventional particulate carbon-black filler (for example, used for the study in Ref. [68]), the conductive composite will have mechanical properties similar to the gel, namely, large deformation with low hysteresis in loading, as shown in Figure 11c for a gel of tetraalkoxysilane with a star silane.[77]

The combination of properties (1) and (2) will lead to a large dynamic range where the composite can be reversibly deformed over large strains with a monotonic increase in conductivity. Lastly, the alignment of the CNT orthogonal to the plane will reduce the ratio X, thus leading to better resolution (see Section 3.1.2). The strength of the method is that it uses an established fabrication process and signal processing method, similar to previous studies (Section 3.1.1). As the film is a gel rather than an elastomer, the background signal arising from bending stress may be significantly lower. This property is critical for applications in surgery and robotics, where the tactile sensor (thin film) will most likely be on a curved surface, such as a robot finger.

Advances in fabrication techniques (such as self-assembly of molecular monolayers over large areas and the robust interconnection of electrodes at a molecular level) in molecular electronics and nanomaterials have made it possible to design new devices. The sensitivity of the energy-band structure of CNTs and nanowires to the presence of surface charges and electric fields[78,79] has been used in the fabrication of molecular sensors. For example, interfacing a network of CNTs between two electrodes coated with the bacterial cell membrane protein rhodopsin results in a sharp shift of the gating voltage (V_g) threshold (Figure 12a).[80] The shift occurs because of modulation of the Fermi energy level of the CNTs by the dipole of rhodopsin (see inset in Figure 12a). A similar effect has also been shown with silicon nanowires, where binding of a specific antigen to an antibody-functionalized silicon nanowire modulates the current across the wire (Figure 12b).[81,82] The change in current occurs because of the local polarization caused by the charge of the antigen (see inset in Figure 12b).[81] Figure 12c shows a conceptual design of a tactile device pixel based on a similar system. A network of nanomaterial, such as CNTs or silicon nanowires, bridges the gap between two fixed electrodes.[83] The network is interfaced with a thin, flexible, pressure-sensitive layer of ferroelectric polymer (such as poly(vinylidene fluoride), PVDF) that exhibits high polarization.[84,85] A tactile force F modulates the polarization of the ferroelectric layer, which in turn modulates the Fermi level of the nanonetwork and registers a signal in the form of a change in current I between the two electrodes. Thus, a a plot of the I values of the individual pixels should generate the surface profile of F. The proposed tactile device will have low power consumption, and its resolution will be decided by the spacing between the electrodes.

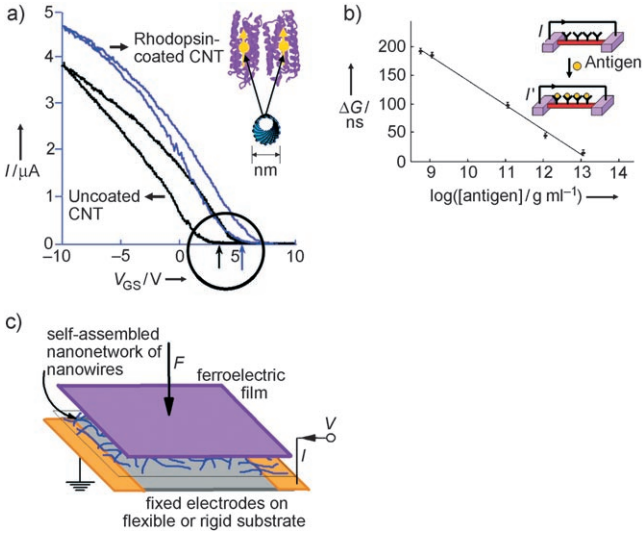

Figure 12. a) Transistor characteristics of uncoated CNTs (black curve) and of CNTs coated with the bacterial cell membrane protein rhodopsin (blue curve). The coating results in a shift in the gate threshold voltage V_{GS} (see arrow in marked area). The inset shows the gating of a CNT by the dipole of rhodopsin.[80] b) Change in conductance G of an antibody-modified silicon nanowire on exposure to different concentrations of an antigen solution. The inset shows a schematic representation of how the binding of the antigen to antibodies results in a change in the current from I to I'.[81] c) Schematic representation of a tactile pixel with a nanonetwork of CNTs or nanowires between two electrodes gated by the polarization of a ferroelectric film. The touch force F modulates the polarization, and thus altering the gating potential, and is registered as the change in current I. Figure 12a reprinted with permission from Ref. [80]. Copyright American Chemical Society. Figure 12b reprinted with permission from Ref. [81]. Copyright Nature Publishing Group.

The capacitance devices (Section 3.1.1) can be significantly improved by the self-assembly of molecules with large (permanent) dipole moments that orient on deformation. The induced dipole orientation tends to dominate (by a factor of ca. 100) over the capacitance change caused by small deformation [given by Eq. (4)]. A monolayer of aligned poly(γ-benzyl-L-glutamate) (PBLG) polarizes as a result of dipole orientation because of accordion-like deformation of the α helix.[86] Although its piezoelectric effect, that is, polarization on deformation, is 30 and 300 times lower than conventionally used materials such as PVDF and lead zirconate titanate (PZT), respectively, its effectiveness of response at low voltages (because of a low ε_r value) compensates for the poor polarization compared to PZT and PVDF.

Highly flexible elastomers with ferroelectric liquid-crystalline polymers is another class of materials that can be reversibly deformed with high strains above 10%, with the change in the polarization caused by a change in the tilt of the

ferroelectric liquid-crystalline molecules.[87] The advantage of a ferroelectric elastomer is the ease of making (and depositing) freestanding thin films (on the scale of tens of nm) compared to ceramic piezoelectric materials.

3.2. Tactile Devices from Materials with Special Chemical Structure

We define "active material" tactile sensors as systems where the transduction is performed by a material with a special molecular or crystalline structure that responds to the local strain by generating a measurable electrical or optical signal. Section 3.2 is divided into three parts: in the first two parts we discuss the commonly used materials, and in the third we speculate on potential high-performance devices based on new findings.

3.2.1. Piezoelectric Materials

Piezoelectric materials are insulators that develop a potential gradient when they are mechanically deformed (strained).[88–90] The property can arise in two ways: 1) From the crystal structure of the material (such as ZnO), where deformation causes the cations and anions to move asymmetrically, thus leading to a high polarization[91] and 2) alignment of the (large) permanent dipole moment of the molecules forming the crystal.[84] The piezoelectric effect arising from the crystal structure usually occurs in inorganic materials, such as $BaTiO_3$, the lead zirconate titanate class of ceramics ($Pb(Zr_xTi_{1-x})O_3$, PZT), ZnO, and CdS.[60,92,93] The molecular effect is observed for macromolecules that have intrinsic permanent dipole moments, such as PVDF, nylon, and PBLG.[84,86]

A typical tactile sensor element or pixel has the same construction as the capacitance-based system (Figure 6), where the dielectric material is a piezoelectric film of thickness D and area A. The film deforms by ΔD on touching with contact force F to generate charges $+Q$ and $-Q$ at the two electrodes.[63,94–96] As the element is also a capacitor, the induced charge leads to a potential V across the pixel, as given by Equation (5), where d is the piezoelectric constant of the material. Strictly speaking, d is a tensor, and the relative orientation of the crystal in the film must be considered. For the simple uniaxial case considered above (and most often used) the tensor notation of d would be d_{33}.[60,97] Similar to the capacitance-based device [Eq. (4)], the sensitivity of response to the applied contact force F is proportional to the signal V. However, in contrast to the capacitance device, the value of D should be large and that of ε_r should be low. In other words, to achieve high sensitivity, the d/ε_r ratio of the piezoelectric material must be as large as possible.

$$V = \frac{dD}{4\pi\varepsilon_r\varepsilon_0 A}F \tag{5}$$

A wide variety of materials, including polycrystalline materials (for example, PZT, ZnO, and PVDF), have been used to make tactile devices. As the material is not perfectly oriented in most fabrication processes to achieve maximum polarization (because of strain) in the direction orthogonal to the film plane, it is "poled; in this way the value of d is increased to the maximum that is practically feasible. The orientation of the dipoles is accomplished in the poling process by applying a strong electric field or by a mechanical process, such as solution casting and shearing.[60]

PZT and PVDF are the materials of choice for tactile sensing because of the requirements for high sensitivity, ease of fabrication, and mechanical properties. In particular, PZT has a higher piezoelectric constant ($d_{33} = 117\ pCN^{-1}$) than single-crystalline materials such as quartz ($d_{11} = 2.3\ pCN^{-1}$) and zinc oxide ($d_{33} = 12\ pCN^{-1}$), and additives can be used to alter its electrical and mechanical properties.[60] PVDF has a lower piezoelectric constant ($d_{33} = 30\ pCN^{-1}$), but its much lower ε_r value (100-fold lower than PZT) makes it an ideal material to make tactile devices.[84] The low cost and ease of processing the polymer (compared to ceramics) has also led to its wide use as a piezoelectric material. A resolution (defined from pixel size) of 0.7 mm has been demonstrated by using PVDF as the filler with sensing forces in excess of 100 KPa.[95] Furthermore, by cross-linking with electron radiation, PVDF-based copolymers have been tailored to operate reversibly up to strains as large as 4%, while in ceramics the strains are limited to well below 0.5%.[98]

Similar to ultrasound imaging in medicine, where local pressure is measured as the damping of the amplitude of oscillations produced by a piezoelectric crystal, tactile devices have been designed as an array of piezoelectric crystal oscillators. The schematic construction of a pixel is similar to that shown in Figure 6. The oscillation of the top electrode relative to the stationary bottom electrode is at maximum at the resonance frequency f_0 of the AC bias. The resonance frequency shifts linearly on application of F. These devices are, in general, less noisy and more sensitive than static devices; however, they are more prone to hysteresis.[92]

3.2.2. Piezoresistive Materials

One of the first ideas on how to measure local strain and stress is based on strain gauges that rely on the change in the electrical conductivity on deformation.[99] Piezoresistive materials are metals and semiconductors where the resistivity of the material ρ modulates on deformation. For semiconductors, the strain modulates the energy of the band gap and the mobility of the charge carriers (electrons and holes). As conductivity (and resistivity) is proportional to the mobility and the density of the charge carriers (which depends exponentially on the band gap), it modulates significantly because of the strain. The dominant effect in semiconductors is the modulation of the band gap between the valence and conduction bands. In metals, the effect is not as dramatic, because the change in the mobility of the electrons with strain is not as significant.[99,100] Although metals (as gauges of metal strain) are commonly used in tactile devices, semiconductor materials are more sensitive to deformation.[99,101–103]

By using the same construction as shown in Figure 6, the relative change in resistance with compressive strain $\Delta D/D$ in the direction perpendicular to the film plane as a consequence

of force F is a linear relationship described by Equation (6).[99,104] Here Π is the effective piezoresistance coefficient perpendicular to the plane of the film, Y is the modulus, and $K_s = \Pi Y$ is the gauge factor that quantifies the sensitivity of the device. Similar to the piezoelectric constant d, Π is a tensor and depends on the orientation of the strain tensor relative to the crystallographic planes of the material.[99] The larger the value of Π (or K_S), the higher is the sensitivity. Metals have K_s values of 2–5, while the values are greater than 150 along the 111 direction for germanium and silicon; thus semiconductor-based devices are significantly more sensitive.[100,101,103–105]

$$\frac{\Delta\rho}{\rho}(\approx\frac{\Delta R}{R}) = \frac{\Pi}{A}F = (\Pi Y)\frac{\Delta D}{D} \quad (6)$$

A high sensitivity to deformation is the key to building potential tactile sensors (and other systems) based on piezoresistive elements. Tactile devices are fabricated by making an array of piezoresistive elements, where each element (pixel) senses the local load. The piezoresistive elements are usually embedded in a soft polymer layer for protection and to make the element compliant to loading. A plot of the change in resistance over the array generates the touch (pressure) image.[101,103]

Figure 13a shows a tactile scanner consisting of a piezoresistive array with a resolution of 1.5 mm that is used for imaging malignant tumors in breasts (Figure 13b). The device is more accurate than ultrasonography in quantifying the tumor size (Figure 13c).[106]

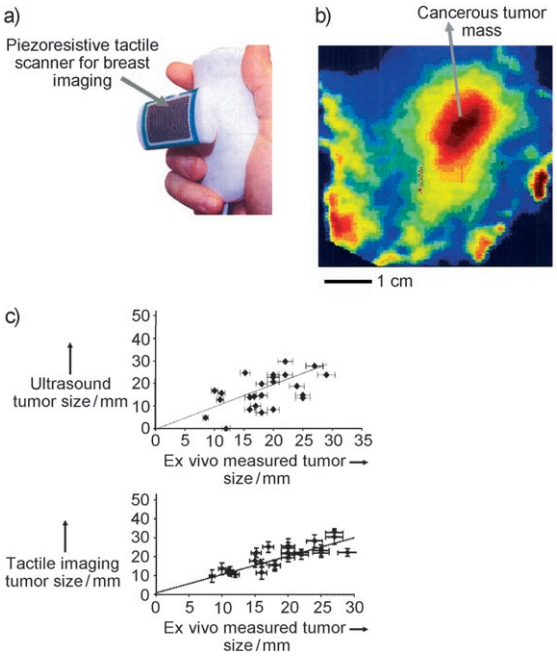

Figure 13. a) A piezoresistive tactile head for scanning across the breast surface to decipher and quantify tumor mass.[106] b) Tactile image of a cancerous tumor mass (infiltrating ductal carcinomas) generated by scanning the breast with the piezoresistive tactile head; the tumor is stiffer than surrounding breast tissue.[106] c) A comparison of the accuracy of tactile imaging and ultrasonography in estimating tumor size.[106] Top: Plot showing the tumor size estimated from ultrasonography and the actual size (from ex vivo measurements); bottom: similar plot but using tactile imaging; ——: identical value. The lower spread of data illustrates the more accurate measurement by tactile imaging. Reprinted with permission from Ref. [106]. Copyright American Medical Association.

3.2.3. *Construction of Highly Sensitive Tactile Devices with Nanostructured Materials and Single-Molecule Properties*

CNTs are interesting materials for designing sensitive tactile devices, not only because of their electrical properties but also because of their electromechanical characteristics.[107] CNTs aligned perpendicular to substrate surfaces are well known for their super compressibility and have now been demonstrated to be highly pressure-sensitive materials (Figure 14a).[108,109] The axial conductivity of an aligned CNT on applying a load parallel to the CNT wall increases monotonically and reversibly up to a compressive strain of 50% (Figure 14b).[109] Thus, a simple device (Figure 14d) can be made by placing an approximately 3.5 mm thick film of well-aligned CNTs between two electrodes (by using a well-established fabrication process[108]). At a fixed bias V the current will modulate as a function of the applied contact force F. A high-resolution, high-sensitivity tactile device can be built, where the current for each pixel is mapped, similar to previous devices (Section 3.1.1).

As indicated earlier, although the piezoelectric constant for ceramic ferroelectric materials is large, their two orders of magnitude higher dielectric constant and modulus compared to PVDF make them less attractive for tactile devices. An interesting possibility may be the use of ZnO nanowires perpendicular to the electrode surface.[110,111] The nanostructure results in the d_{33} value being enhanced by about 50% (from 13 to 20 pCN^{-1});[112] however, more interestingly, the modulus is reduced from 140 GPa for bulk ZnO to about 35 GPa for ZnO.[111] A typical design may be similar to a CNT-based device (Figure 14d), where the nanowires perpendicular to the electrode surface (Figure 14e) are sandwiched between the electrodes. The application of a contact force F will cause a potential difference V between the two electrodes[113] that can be analyzed, similar to piezoelectric devices (Section 3.2.1), by imaging the contact force distribution over an array of pixels.

A further miniaturization is possible when the nanostructure materials, such as CNTs and ZnO nanowires, are replaced, for example, by a molecular device composed of a molecular monolayer of pressure-sensitive molecules (Figure 15a). Recently, it has been shown what has long been conjectured, that conductivity along the main axis of the molecules is sensitive to the conformation of the molecule.[114] Since this first demonstration, modulation of (single molecule) conductance G by deformation has been reported.[115,116] A study of a series of alternating $(benzene\text{-}furan)_n$ oligomers (where $n = 1$–4; Figure 15b) that are flexible and contain 6–18 conjugated double bonds to allow conduction has demonstrated a 40–75% change in conductance as a result of deformation.[115] Although the change in conductance for $n = 2$ (see Figure 15c) because of deformation is about 25%, the

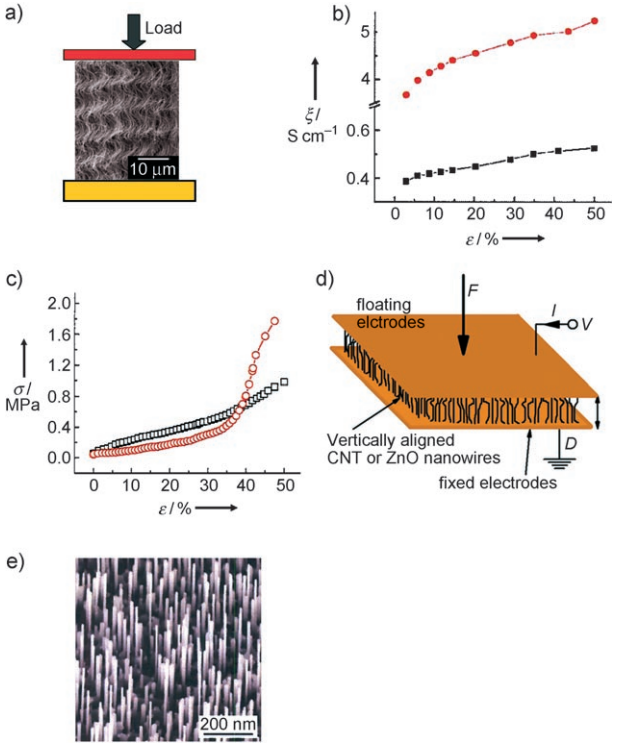

Figure 14. a) CNTs aligned perpendicular to the substrate are deformed on applying a load parallel to the CNT walls, as seen by the undulations in the CNT in the scanning electron micrograph.[108] b) The conductivity of the CNT structure increases monotonically with strain, and a higher sensitivity is observed for compressive loading parallel to the CNT walls (●) compared to perpendicular loading (■).[109] c) The CNT structure of both parallel (○) and perpendicular loading strains (□) compresses rapidly on application of stress; the low modulus leads to a higher sensitivity than bulk polymer films.[109] d) Schematic representation of a tactile pixel made with vertically aligned CNTs or ZnO nanowires of length *D*. The current *I* modulates on application of tactile force *F* to the device. A map of change in *I* over all the pixels will generate the tactile image of *F*. e) An SEM image of vertically aligned ZnO nanowires grown on an aluminum oxide substrate.[111] Figure 14 a–c reprinted with permission from Ref. [108]. Copyright American Institute of Physics. Figure 14 d reprinted with permission from Ref. [111]. Copyright American Chemical Society.

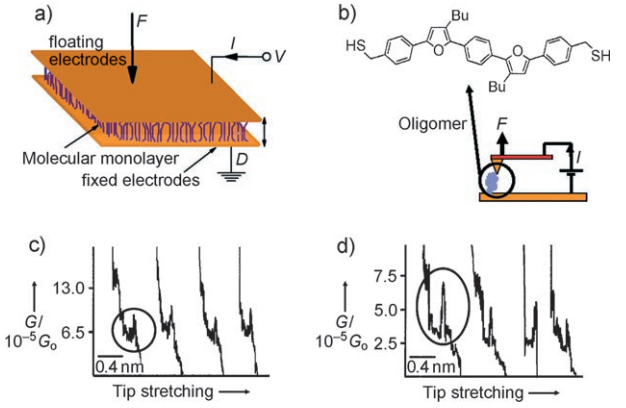

Figure 15. a) Schematic representation of a molecular electronic based tactile pixel. The tactile force *F* changes the conformation of molecules in the pixel, thereby modulating the current *I* through the molecules and, hence, the device. b) Chemical structure of a $(\text{benzene-furan})_n$ oligomer ($n=2$).[115] The inset shows the conductance measurement setup where an oligomer molecule bridges the gap between a scanning tunneling electron microscope (STM) tip and the substrate. The tip is pulled away from the substrate, thereby stretching the oligomer, and the change in conductance is measured with the stretching distance. c) The change in conductance *G* (measured in units of the fundamental conductance unit $G_0 = 2e^2/h$, ca. 77.4 μS) of the $n=2$ oligomer as a function of the distance between the gold substrate and the STM tip.[115] The circles highlight the change in conductance observed for the oligomer on stretching. The picture shows four conductivity traces for the oligomer. d) Similar conductivity traces for the $n=3$ oligomer.[115] The relative change in conductance *G* is higher than for the $n=2$ oligomer but is more abrupt. Figure 15 b–d reprinted with permission from Ref. [115]. Copyright The Royal Society of Chemistry.

change is less abrupt than for $n=3$, which has a change of about 75% (Figure 15 d).[115]

A reliable method to place the top electrode (Figure 15 a) in order to form a robust electrical interconnection is required to enable large-area molecular-electronic devices to be built on this principle. Although the molecular electronic devices are far from commercialization, an interesting method, in which a conducting polymer is used as the top electrode (followed by deposition of a metallic electrode), recently demonstrated the possibility of making large-area robust (electrical) junctions between single molecules and the electrode.[117]

Optical devices, which use interference phenomena, may offer an alternative strategy to electrical transduction. Tactile devices based on the modulation of Bragg grating have been demonstrated;[118] however, the possible routes to improve resolution below 1 mm and to make large-area devices are difficult. Nanostructure photonic materials made from self-assembled block copolymers may be attractive alternatives. Recently, it was demonstrated that block copolymer gels from styrene and 2-vinylpyridine form (self-assembled) stacks of lamella parallel to a film surface and that these were effective materials for determining the local strain as seen by measurement of the optical interference.[119] These one-dimensional photonic crystals show an approximately 575% change in the peak position wavelength (namely, the stop band), namely, from the UV/Vis to infrared region at nominal strain. Directly recording the color interference pattern on a digital camera as a function of wavelength to image the strain distribution on touch may lead to a high-resolution device with a large array. A resolution of about 1 μm in the visible range may be possible, depending on the strength of the light source used to achieve the interference pattern. The advantage of this approach is that the optical signal can be acquired directly on a digital camera, whereas fiberoptics-based systems may become complex and expensive for imaging over a large area of contact.

Furthermore, the over 50-fold enhancement in the piezoresistive coefficient of silicon nanowires compared to bulk silicon may be explored to make a clever design for tactile devices.[120]

4. High-Resolution Tactile Sensor

The current tactile devices based on the principles described in Section 3 have two main limitations to make a significant impact in robotics, surgery, and cancer detection (Section 1): 1) The resolution for a device with a contact area greater than 1 cm^2 is about 1 mm[3] compared to 40 μm[1] for a human finger, and 2) the devices are made on a flat substrate, and thus there will be a significant non-uniform background signal arising from (residual) stress caused when bending them over a curved surface to emulate a finger of a robot or a surgical device. In this section, we describe a recently developed device that has a resolution on a par with a human finger and can be directly fabricated on a curved surface to avoid the large background signal caused by residual stress.[121]

A five nanoparticle monolayer structure separated by dielectric layers has been constructed on a transparent indium-tin-oxide (ITO) electrode by using the well known layer-by-layer self-assembly technique[121] (Figure 16).[122] The

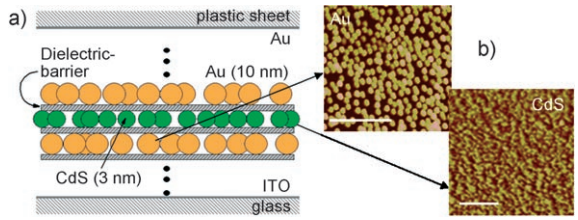

Figure 16. Multilayer structure of an electrooptical device. a) Schematic representation of the tactile device showing the nanoparticle monolayers spaced by the organic dielectric layers that are made of four monolayers each of PSS and PAH.[122] b) AFM topography image after subsequent deposition of the first Au layer and the first CdS layer. Scale bar: 100 nm.

dielectric layer is approximately 5–6 nm thick film composed of a total of four alternating monolayers of poly(allylamine hydrochloride) (PAH) and poly(styrene sulfonate) (PSS). The nanoparticles are well below the percolation threshold in the in-plane direction and, therefore, are not conducting; while the film is conducting in the direction perpendicular to the plane because the electrons can tunnel through the dielectric barrier. Electric current flows through the film on application of a bias V across the film, and the CdS nanoparticles emit visible light at a wavelength of 580 nm (the electroluminescence light). The application of load L to the top of the Au/plastic electrode (see Figure 17) causes the dielectric layer to become compressed and the particles to get closer together, thus causing an increase in both the local current density J and the electroluminescent light I_{EL}. The local stress distribution obtained by pressing, for example, an Indian 5 Rupee coin (Figure 17), on the surface can be directly recorded on a digital camera as a "stress image" (Figure 17). Further analysis of the device using a grid with lines about 40 μm wide indicates that the resolution is higher than 20 μm.[122]

To measure the device characteristics, an optically smooth quartz disk 2.5 cm in diameter was pressed on the device such

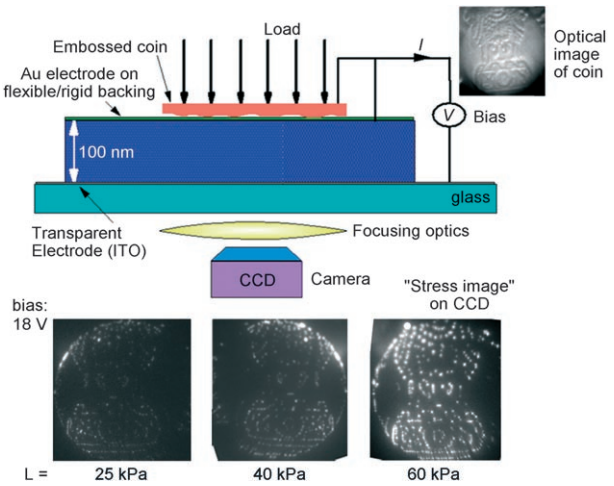

Figure 17. Pressing a coin on the surface of the device generates its electroluminescence image on the CCD, from the stress image (as a result of embossing on the coin). The intensity of the image increases with load. The images were taken at a bias of 18 V.

that the average load L was constant over the area of contact, thereby leading to uniform I_{EL} (Figure 18a).[122] The current density J is obtained by dividing the current by the area of contact. The load and bias conditions are below 100 KPa to avoid current enhancement from the edges caused by the hole-punch effect[123] (Figure 18b). The J–V characteristics

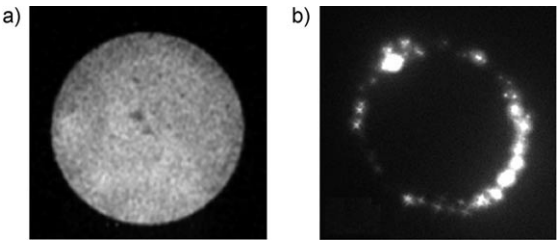

Figure 18. The hole punch effect observed at high biases/stresses. a) Stress image of an optically flat quartz disk of diameter 2.5 cm at $V = 18$ V and 40 KPa loading.[122] b) The same stress image at 100 KPa, indicating enhancement of electroluminescence at the edges as a result of the hole-punch effect.[122]

are consistent with the expectation that as L increases, the particles will be pushed closer together to cause an increase in the J value (Figure 19). At a given value of V, J is given by a combination of the ionic current J_I, which follows Ohm's law, and the tunneling current J_T, which is given by the Fowler–Nordheim equation. The ionic current is attributed to the ions in the polyelectrolyte that will migrate because of the applied field. The tunneling current between the adjacent nanoparticles is due to electron transport through the polymer barrier. Thus, the total current density is given by Equation (7).[122] The ionic resistance R is inversely proportional to ion mobility, $P(V) \approx V^2$ is proportional to the number density

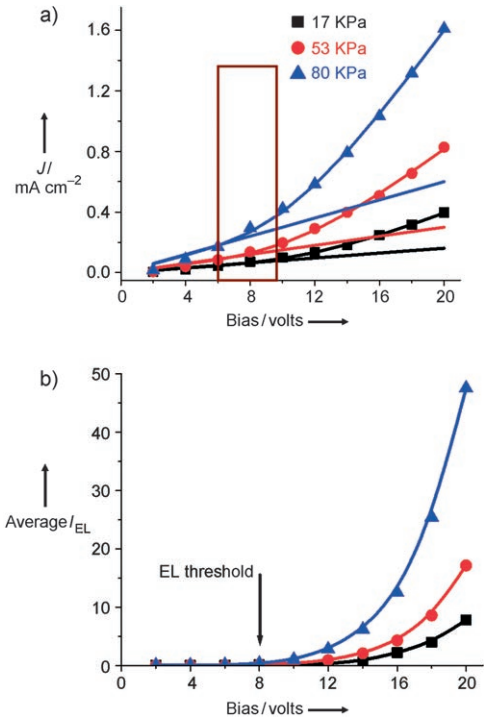

Figure 19. Electrooptical characteristics of the device and electron-transport mechanism. The device is compressed using an optically flat quartz disk on the flexible Au electrode. The *J*–*V* and I_{EL}–*V* characteristics are measured at a fixed load *L*. a) The fitted line is based on a model combining charge transport by electron tunneling (J_T) and ions (J_I) given [Eq. (7)]. The straight line corresponds to J_I. Rectangle: Electron tunneling begins.[122] b) The start of electroluminescence I_{EL} from the device matches the bias where *J* begins to deviate from linearity, that is, the value of J_T becomes significant.[122]

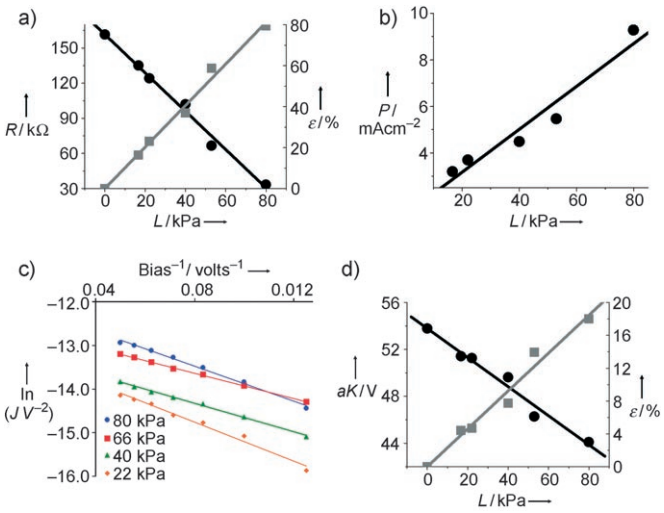

Figure 20. The electrical characteristics of the device from fitting the *J*–*V* characteristics based on Equation (7). a) The ionic resistance *R* (●) decreases linearly with load, and the calculated strain (■) shows an elastic response from the film.[122] b) The number of tunneling channels *P* increases linearly with load. c) Confirmation of field-assisted electron tunneling as $P \approx V^2$. d) The tunneling barrier *aK* decreases linearly with load, signifying deformation of the dielectric films between the nanoparticles on local compression (■).[122]

of free electrons, *a* is the (vertical) distance between particles, and *K* is the critical field for activated electron tunneling.

$$J = J_I + J_T = \frac{V}{R} + P(V)\exp(-\frac{aK}{V}) \quad (7)$$

Equation (7) gives an excellent description of the *J*–*V* results from the device (Figure 19a). The device characteristics can be divided into two regions: a) Low bias: a straight line is obtained at low bias where the field-assisted tunneling is insignificant because the electric field is low. The current is dominated by ionic transport J_I. The value of *R* can be estimated from the slope of the fitted line in Figure 19a for the *J*–*V* curve at each value of *L* [Eq. (7)]. b) High bias: As the bias increases, the field-assisted tunneling begins to dominate, which makes the relationship between *J* and *V* nonlinear. The *aK* and *P* values are obtained from the fitting results at different values of *L*. The device shows a threshold in electroluminescence (Figure 19b) that corresponds to the initiation of electron tunneling at a bias above 8 V (Figure 19b).

Figure 20a shows the estimated value of *R* as a function of *L* from the fits in Figure 19.[122] As *R* ~ thickness of the film at a constant area, defined by the quartz disk, the compressive strain of the film can be estimated as $\varepsilon_F(L) = [R(L=0) - R(L)]/R(L=0)$. Both *R* and ε_F are a linear function of *L*, and the deformation of the film is reversible. The linearity is observed up to 80% strain, thus indicating that the range of deformation in the experiments is reasonably broad.

The front factor *P* for J_T in Equation (7) is proportional to the number of charge carriers in the conducting media. The value of *P* is a constant for a slab of conductor at a constant temperature. Not all particles in a composite are involved in electron transport and, thus, *P* is proportional to the number of particles participating in the conduction. In other words, *P* can be considered as the effective number of channels that percolate the electrons between the two electrodes. Figure 20b shows, as expected, that the number of percolating channels increases with load because the particles come closer together to make more contact in the direction perpendicular to the film.[122] If the linear, ionic component is then subtracted from Equation (7), $\ln[J_T/V^2] \approx 1/V$, which is consistent with the Fowler–Nordheim model on field-assisted tunneling that states $P \approx V^2$. The linearity of the plot in Figure 20c confirms the validity of the transport by field-assisted electron tunneling.

Figure 20d shows the behavior of the tunneling barrier parameter *aK* as a function of *L*.[122] As the load increases, the particles are expected to come closer together and result in a decrease in the tunneling barrier because the same (interparticle) potential is applied over a shorter distance, thus causing a higher electric field through the dielectric layer. Thus, similar to the value of *R*, it is possible to calculate "local compressive strain" of the dielectric film, $\varepsilon_L = [aK(L=0) - aK(L)]/aK(L=0)$ from the change in the interparticle distance *a*. Similar to the film (Figure 20a), the local strain is

linear with respect to L. However, the strain is significantly lower.

Figure 21 compares the local (ε_L), that is, compression of the dielectric layer, and overall (ε_F) mechanical deformation

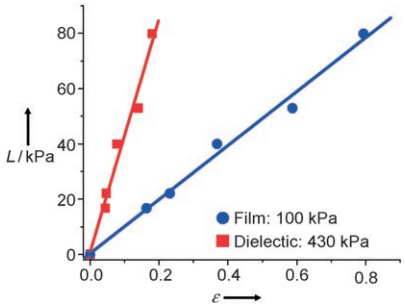

Figure 21. The mechanical properties of the device. The local strain ε_L (compression of the dielectric barrier) and overall strain ε_F (compression of the whole film) is obtained from the electrical properties.

of the film. There are three characteristics: 1) The overall modulus of the film is very low; 2) the total strain is very large, well over 10% for local and 50% for total deformation (namely, the film); and 3) the local (namely, dielectric) modulus is significantly larger than the overall modulus of the film. The deformation is counterintuitive because squeezing thinner polymer film requires significantly (exponentially) larger force than a thicker film.[124] This observation can be explained by considering the film to be a nanofoam as a result of the non-uniform deposition of the polymer on the nanoparticles leaving voids in the interparticle region. The low modulus and large observed strains can be attributed to the easy deformation of the voids. The non-affine deformation is attributed to the well-known property of foams in which two types of strain occur: the deformation of the voids and bending/stretching of the matrix.[125] Furthermore, because the polyelectrolytes are hygroscopic with a large water content (consistent with high J_I), the matrix may be a gel and sustain large strains. The low modulus of the film and reversibility up to 80% strains makes the device highly sensitive to touch, with a resolution on a par with a human finger.

Instead of measuring the electroluminescent light, the stress distribution can be obtained by measuring the local current density distribution in a configuration similar to a liquid-crystal display (Figure 22). Typically, at a bias of 25 V for a load of 10 KPa, a current density of at least $J = 0.1\ \mathrm{mA\,cm^{-2}}$ is generated that is fairly stable.[122] Based on a conservative estimate of 1 nA as a minimum measurable current, the area of the intersection would be, 32 μm^2. Thus, a resolution of 40 μm, comparable to a human finger, can be achieved with this electrical device with no optical components.

Finally, as mentioned in Section 2, the viscoelasticity of skin improves the characteristics of tactile sensing by enhancing the response to load and reducing the energy requirement. We have investigated the dynamic response of the tactile device by observing the transient responses in I_{EL} and J to step modulation in stress. Preliminary results show a

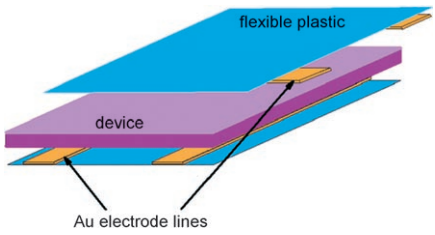

Figure 22. An electronic tactile sensor device. Instead of measuring the I_{EL} value, the current density distribution can be measured by having the electrodes as strips, as shown above. The current at the "intersection" defined by the strip geometry can be obtained by sequentially biasing the top and bottom set of strips.[122]

viscoelastic type response in J and I_{EL} on application of a square-wave modulation in stress to the device (Figure 23). The response is similar to that of the stress response

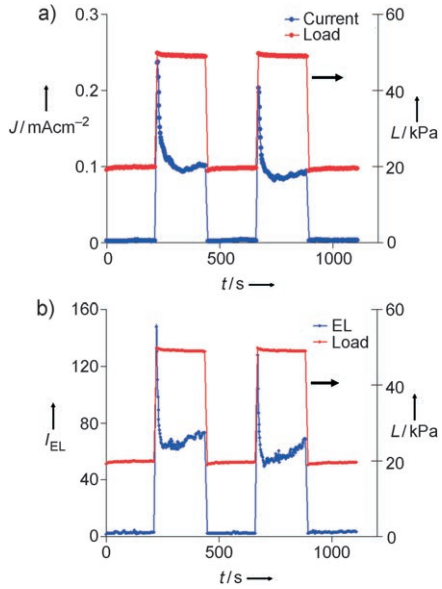

Figure 23. Application of a square-wave stress modulation to the device results in a) J and b) I_{EL} showing a response characteristic of a viscoelastic material. A sharp increase in the J and I_{EL} values at the edges of the stress waves is followed by an exponential decay to a stable value.

(Figure 1a) of the viscoelastic element (Figure 1a and 3c). A sharp offshoot in both J and I_{EL} is observed at the edge of the square stress waves. The offshoot decays on the time scale of seconds to a stable response. The viscoelastic-type response is promising in providing information on the rate of strain, hence, mimicking human skin unlike any other reported tactile sensor.

5. Summary and Outlook

Emulating touch on a par with a human finger will play a key role in the development of humanoid robots and significantly improving the sophistication and performance of minimally invasive surgery. Although highly successful and

effective tactile devices have been designed and made over the last three decades, they differ from the natural device in two aspects that, in our opinion, are critical challenges to overcome prior to making a quantum jump in performance and solving some of the basic limitations (such as high curvature devices and very large area devices).

1. The tactile device element: A fundamental difference (and perhaps the hardest materials-related challenge) between all of the current device elements and neurons is that the natural device is intrinsically digital, with the frequency of neural firing (pulse) being proportional to the intensity of the stimuli, while the current artificial devices are analogue. The development of a novel material that will allow an intrinsic digital response to stimuli will significantly improve device sensitivity and the signal-to-noise ratio. Furthermore, similar to nature, a tactile device with a variety of sensors that specialize in terms of speed, sensitivity, and resolution (Table 1) will significantly improve the quality of tactile information. For example, instead of the single type of sensor element currently used in tactile devices, a combination of near- and far-field sensors with slow and fast responses would solve some of the limitations, such as dynamic sensing and discerning texture.

2. Viscoelasticity and dynamic sensing: Similar to the dermis, integrating the viscoelastic property of a material into the tactile device may significantly enhance our currently poor capability of "feeling" motion during touch or using relative velocity between the sensor and the body surface to enhance the quality of (texture) sensation. A viscoelastic matrix that transmits the signal to the imbedded sensor, although passive, can "translate" a dynamic response to physical features (Figure 3), such as when the boundaries of the texture are significantly enhanced because of stress relaxation. A straightforward mimicry would require designs where the stimuli reaching the sensor element transmits through a viscoelastic medium. Another possible route may be to make the active device element itself viscoelastic (Figure 23).

The recent developments in materials chemistry, nanostructures, nanodevices, and single-molecule devices have great potential in improving the current technology significantly. Some potential developments are discussed in Sections 3.1.3 and 3.2.3. Current methods using a pressure-sensitive elastomer can be significantly improved by replacing the conventional carbon-black filler with CNTs to improve the sensitivity, resolution, and dynamic range of the device, because the very large length/diameter ratio of the CNTs changes the percolation behavior of the composite significantly (Figure 11). The electronic properties of CNTs and semiconducting nanowires as stand-alone transistors (where the current can be gated by small modulations in the voltage over the length of the wire or tube) opens up the possibility of designing high-resolution, low-energy tactile devices integrated with self-assembled piezoelectric films (Figure 12a). Pressure-sensitive nanomaterials, such as piezoresistive CNTs and piezoelectric ZnO, can be used to design nanodevices and molecular devices (Figure 14). Molecular devices using deformation-induced modulation of single-molecule conductance in certain molecules can be used to build tactile devices by self-assembly processes (Figure 15). An interesting aspect of some nanomaterials-based devices (not possible for current micrometer-scale devices) is their relatively inexpensive processing under ambient conditions and the ability to directly make large-area devices on curved surfaces. This advantage is explicitly demonstrated in the nanodevice discussed in Section 4, where an improvement in the resolution by two orders of magnitude over current technology is achieved. The device is built at ambient conditions using wet chemistry.

R.F.S. thanks the National Science Foundation (grant CMMI-0740044) and the US Army-Robert Morris Acquisition Center (grant W911NF-04-2-001) for their generous financial support. We thank Trisia Fenster for making the frontispiece illustration.

Received: August 12, 2007
Revised: February 4, 2008

[1] J. W. Morley, A. W. Goodwin, I. Darian-Smith, *Exp. Brain Res.* **1983**, *49*, 291 – 299.
[2] S. A. Mascaro, H. H. Asada, *IEEE Trans. Rob. Autom.* **2001**, *17*, 698 – 708.
[3] T. Someya, T. Sekitani, S. Iba, Y. Kato, H. Kawaguchi, T. Sakurai, *Proc. Natl. Acad. Sci. USA* **2004**, *101*, 9966 – 9970.
[4] P. N. Brett, R. S. Stone, *Proc. Inst. Mech. Eng. Part H* **1997**, *211*, 309 – 316.
[5] S. Matsumoto, R. Ooshima, K. Kobayashi, N. Kawabe, T. Shiraishi, Y. Mizuno, H. Suzuki, S. Umemoto, *Surg. Endosc.* **1997**, *11*, 939 – 941.
[6] P. K. Plinkert, I. Baumann, E. Flemming, *Laryngorhinootologie* **1997**, *76*, 543 – 549.
[7] N. Sakai, M. Tatsuta, H. Yano, H. Iishi, S. Ishiguro, *Gastrointest. Endosc.* **2000**, *51*, 69 – 73.
[8] O. Tohyama, S. Maeda, H. Itoh, *IEEE J. Sel. Top. Quantum Electron.* **1999**, *5*, 115 – 118.
[9] A. Zangaladze, C. M. Epstein, S. T. Grafton, K. Sathian, *Nature* **1999**, *401*, 587 – 590.
[10] G. Robles-De-La-Torre, V. Hayward, *Nature* **2001**, *412*, 445 – 448.
[11] Y. Murayama, C. E. Constantinou, S. Omata, *Sens. Actuators A* **2005**, *120*, 543 – 549.
[12] X. C. Jin, O. Oralkan, F. L. Degertekin, B. T. Khuri-Yakub, *IEEE Trans. Ultrason. Ferroelectr. Freq. Control* **2001**, *48*, 750 – 760.
[13] B. Gates, *Sci. Am.* **2007**, *296*, 44 – 51.
[14] R. Crowder, *Science* **2006**, *312*, 1478 – 1479.
[15] P. Dario, E. Guglielmelli, C. Laschi, *J. Robot Syst.* **2001**, *18*, 673 – 690.
[16] Y. B. Jia, *IEEE Trans. Rob. Autom.* **2005**, *21*, 726 – 733.
[17] A. M. Okamura, M. R. Cutkosky, *Int. J. Robot. Res.* **2001**, *20*, 925 – 938.
[18] Y. Okumura, T. Tawara, T. Furuta, K. Endo, M. Shimizu, M. Shimomura, H. Kitano, *Adv. Robot.* **2004**, *18*, 699 – 710.
[19] M. Shikida, T. Shimitzu, K. Sato, K. Itoigawa, *Sens. Actuators A* **2003**, *103*, 213 – 218.
[20] A. Bicchi, V. Kumar, *IEEE Int. Conf. Robot. Autom.* **2000**, 348 – 353.
[21] M. J. Mack, *JAMA J. Am. Med. Assoc.* **2001**, *285*, 568 – 572.
[22] M. H. Lee, *Int. J. Robot. Res.* **2000**, *19*, 636 – 643.
[23] E. D. Adrian, *The Basis of Sensation*, Norton, New York, **1928**.
[24] S. J. Bolanowski, Jr., G. A. Gescheider, R. T. Verrillo, C. M. Checkosky, *J. Acoust. Soc. Am.* **1988**, *84*, 1680 – 1694.
[25] P. G. Gillespie, R. G. Walker, *Nature* **2001**, *413*, 194 – 202.

[26] J. D. Liu, B. Schrank, R. H. Waterston, *Science* **1996**, *273*, 361 – 364.
[27] K. A. Holbrook, L. T. Smith, *Morphology of connective tissue: structure of skin and tendon*, Wiley-Liss, New York, **1993**.
[28] F. H. Silver, L. M. Siperko, G. P. Seehra, *Skin Res. Technol.* **2003**, *9*, 3 – 23.
[29] J. C. Barbenel, J. H. Evans, *J. Invest. Dermatol.* **1977**, *69*, 318 – 320.
[30] J. M. Pereira, J. M. Mansour, B. R. Davis, *J. Biomech. Eng.* **1991**, *24*, 157 – 162.
[31] F. H. Silver, J. W. Freeman, D. DeVore, *Skin Res. Technol.* **2001**, *7*, 18 – 23.
[32] D. R. Veronda, R. A. Westmann, *J. Biomech. Eng.* **1970**, *3*, 111 – 124.
[33] J. D. Ferry, *Viscoelastic Properties of Polymers, 3rd ed.*, Wiley, New York, **1980**.
[34] M. D. Ridge, V. Wright, *J. Appl. Physiol.* **1966**, *21*, 1602 – 1606.
[35] F. H. Silver, G. P. Seehra, J. W. Freeman, D. DeVore, *J. Appl. Polym. Sci.* **2002**, *86*, 1978 – 1985.
[36] P. L. Kronick, *Connect. Tissue Res.* **1988**, *18*, 95 – 106.
[37] G. P. Seehra, F. H. Silver, *Skin Res. Technol.* **2006**, *12*, 190 – 198.
[38] H. Oxlund, J. Manschot, A. Viidik, *J. Biomech. Eng.* **1988**, *21*, 213 – 218.
[39] F. H. Silver, D. L. Christiansen, P. B. Snowhill, Y. Chen, *J. Appl. Polym. Sci.* **2001**, *79*, 134 – 142.
[40] F. H. Silver, A. Ebrahimi, P. B. Snowhill, *Connect. Tissue Res.* **2002**, *43*, 569 – 580.
[41] F. H. Silver, I. Horvarth, D. J. Foran, *J. Theor. Biol.* **2002**, *216*, 243 – 254.
[42] C. H. Daly, G. F. Odland, *J. Invest. Dermatol.* **1979**, *73*, 84 – 87.
[43] W. K. Purves, D. Sadava, G. H. Orians, C. H. Heller, *Life: The Science of Biology, 7th ed.*, Sinauer and Freeman, New York, **2003**.
[44] D. F. Collins, B. Knight, A. Prochazka, *J. Neurophysiol.* **1999**, *81*, 2215 – 2225.
[45] B. B. Edin, G. K. Essick, M. Trulsson, K. A. Olsson, *J. Neurosci.* **1995**, *15*, 830 – 847.
[46] B. B. Edin, *J. Neurophysiol.* **2004**, *92*, 3233 – 3243.
[47] E. Gamzu, E. Ahissar, *J. Neurosci.* **2001**, *21*, 7416 – 7427.
[48] A. Ochoa, E. Torebjork, *J. Physiol.* **1983**, *342*, 633 – 654.
[49] A. B. Vallbo, K. E. Hagbarth, H. E. Torebjork, B. G. Wallin, *Physiol. Rev.* **1979**, *59*, 919 – 957.
[50] R. S. Johansson, *J. Physiol.* **1978**, *281*, 101 – 125.
[51] R. S. Johansson, A. B. Vallbo, *J. Physiol.* **1979**, *286*, 283 – 300.
[52] I. Birznieks, P. Jenmalm, A. W. Goodwin, R. S. Johansson, *J. Neurosci.* **2001**, *21*, 8222 – 8237.
[53] T. Maeno, K. Kobayashi, N. Yamazaki, *JSME Int. J. Ser. C* **1998**, *41*, 94 – 100.
[54] M. A. Srinivasan, J. M. Whitehouse, R. H. Lamotte, *J. Neurophysiol.* **1990**, *63*, 1323 – 1332.
[55] R. S. Johansson, I. Birznieks, *Nat. Neurosci.* **2004**, *7*, 170 – 177.
[56] D. J. Griffiths, *Introduction to Electrodynamics, 3rd ed.*, Prentice Hall, Englewood Cliffs, NJ, **2006**.
[57] W. P. Eaton, J. H. Smith, *Smart Mater. Struct.* **1997**, *6*, 530 – 539.
[58] C. M. Ho, Y. C. Tai, *Annu. Rev. Fluid Mech.* **1998**, *30*, 579 – 612.
[59] J. W. Judy, *Smart Mater. Struct.* **2001**, *10*, 1115 – 1134.
[60] D. L. Polla, L. F. Francis, *Annu. Rev. Mater. Sci.* **1998**, *28*, 563 – 597.
[61] R. E. Oosterbroek, T. S. J. Lammerink, J. W. Berenschot, G. J. M. Krijnen, M. C. Elwenspoek, A. van den Berg, *Sens. Actuators A* **1999**, *77*, 167 – 177.
[62] J. N. Palasagaram, R. Ramadoss, *IEEE Sens. J.* **2006**, *6*, 1374 – 1375.
[63] K. Arshak, E. Jafer, A. Fox, *Compos. Sci. Technol.* **2005**, *65*, 757 – 764.
[64] M. Leineweber, G. Pelz, M. Schmidt, H. Kappert, G. Zimmer, *Sens. Actuators A* **2000**, *84*, 236 – 245.
[65] N. Sato, S. Shigematsu, H. Morimura, M. Yano, K. Kudou, T. Kamei, K. Machida, *IEEE Trans. Electron Devices* **2005**, *52*, 1026 – 1032.
[66] P. A. Schmidt, E. Mael, R. P. Wuertz, *Rob. Auton. Syst.* **2006**, *54*, 1005 – 1014.
[67] Y. M. Shkel, N. J. Ferrier, *IEEE-ASME Trans. Mechatron.* **2003**, *8*, 318 – 325.
[68] J. K. W. Sandler, J. E. Kirk, I. A. Kinloch, M. S. P. Shaffer, A. H. Windle, *Polymer* **2003**, *44*, 5893 – 5899.
[69] R. Zallen, H. Scher, *Phys. Rev. B* **1971**, *4*, 4471 – 4479.
[70] Y. Cao, P. Smith, A. J. Heeger, *Synth. Met.* **1992**, *48*, 91 – 97.
[71] C. A. Martin, J. K. W. Sandler, M. S. P. Shaffer, M. K. Schwarz, W. Bauhofer, K. Schulte, A. H. Windle, *Compos. Sci. Technol.* **2004**, *64*, 2309 – 2316.
[72] K. Weib, H. Worn, *IEEE Int. Conf. Mechatron. Autom.* **2005**, *1*, 471 – 473.
[73] Z. Del Prete, L. Monteleone, R. Steindler, *Rev. Sci. Instrum.* **2001**, *72*, 1548 – 1553.
[74] S. Kiekpatrick, *Rev. Mod. Phys.* **1973**, *45*, 574 – 578.
[75] J. H. Rouse, *Langmuir* **2005**, *21*, 1055 – 1061.
[76] O. Regev, P. N. B. Elkati, J. Loos, C. E. Koning, *Adv. Mater.* **2004**, *16*, 248 – 251.
[77] K. G. Sharp, *J. Mater. Chem.* **2005**, *15*, 3812 – 3820.
[78] R. Martel, T. Schmidt, H. R. Shea, T. Hertel, P. Avouris, *Appl. Phys. Lett.* **1998**, *73*, 2447 – 2449.
[79] H. W. C. Postma, T. Teepen, Z. Yao, M. Grifoni, C. Dekker, *Science* **2001**, *293*, 76 – 79.
[80] K. Bradley, A. Davis, J. C. P. Gabriel, G. Gruner, *Nano Lett.* **2005**, *5*, 841 – 845.
[81] G. F. Zheng, F. Patolsky, Y. Cui, W. U. Wang, C. M. Lieber, *Nat. Biotechnol.* **2005**, *23*, 1294 – 1301.
[82] W. U. Wang, C. Chen, K. H. Lin, Y. Fang, C. M. Lieber, *Proc. Natl. Acad. Sci. USA* **2005**, *102*, 3208 – 3212.
[83] E. S. Snow, J. P. Novak, P. M. Campbell, D. Park, *Appl. Phys. Lett.* **2003**, *82*, 2145 – 2147.
[84] A. J. Lovinger, *Science* **1983**, *220*, 1115 – 1121.
[85] A. V. Bune, V. M. Fridkin, S. Ducharme, L. M. Blinov, S. P. Palto, A. V. Sorokin, S. G. Yudin, A. Zlatkin, *Nature* **1998**, *391*, 874 – 877.
[86] T. Jaworek, D. Neher, G. Wegner, R. H. Wieringa, A. J. Schouten, *Science* **1998**, *279*, 57 – 60.
[87] W. Lehmann, H. Skupin, C. Tolksdorf, E. Gebhard, R. Zentel, P. Kruger, M. Losche, F. Kremer, *Nature* **2001**, *410*, 447 – 450.
[88] M. Born, K. Huang, *Dynamical Theory of Crystal Lattices*, Oxford University Press, Oxford, **1954**.
[89] W. F. Cady, *Piezoelectricity*, McGraw-Hill, New York, **1946**.
[90] J. F. Nye, *Physical Properties of Crystals*, Oxford University Press, Oxford, **1957**.
[91] C. Kittel, *Introduction to Solid State Physics, 7th ed.*, Wiley, Newe York, **1995**.
[92] G. M. Krishna, K. Rajanna, *IEEE Sens. J.* **2004**, *4*, 691 – 697.
[93] D. L. Polla, W. T. Chang, R. S. Muller, R. M. White, *IEEE Inter. Electron Dev.* **1985**, 133 – 136.
[94] J. Dargahi, M. Parameswaran, S. Payandeh, *J. Microelectromech. Syst.* **2000**, *9*, 329 – 335.
[95] E. S. Kolesar, C. S. Dyson, *J. Microelectromech. Syst.* **1995**, *4*, 87 – 96.
[96] W. T. Liu, A. Menciassi, S. Scapellato, P. Dario, Y. Q. Chen, *Rob. Auton. Syst.* **2006**, *54*, 513 – 528.
[97] J. Sirohi, I. Chopra, *J. Intell. Mater. Syst. Struct.* **2000**, *11*, 246 – 257.
[98] Q. M. Zhang, V. Bharti, X. Zhao, *Science* **1998**, *280*, 2101 – 2104.
[99] C. S. Smith, *Phys. Rev.* **1954**, *94*, 42 – 49.
[100] W. P. Mason, R. N. Thruston, *J. Acoust. Soc. Am.* **1957**, *29*, 1096 – 1101.
[101] Y. Hasegawa, M. Shikida, T. Shimizu, T. Miyaji, H. Sasaki, K. Sato, K. Itoigawa, *Sens. Actuators A* **2004**, *114*, 141 – 146.

[102] Y. Hasegawa, M. Shikida, H. Sasaki, K. Itoigawa, K. Sato, *J. Micromech. Microeng.* **2006**, *16*, 1625 – 1632.
[103] T. V. Papakostas, J. Lima, M. Lowe, *Proc. IEEE Sens.* **2002**, *2*, 1620 – 1624.
[104] J. Engel, J. Chen, C. Liu, *Appl. Phys. Lett.* **2006**, *89*, 221907-3.
[105] H. Takao, K. Sawada, M. Ishida, *IEEE Trans. Electron Devices* **2006**, *53*, 1250 – 1259.
[106] P. S. Wellman, E. P. Dalton, D. Krag, K. A. Kern, R. D. Howe, *Arch. Surg.* **2001**, *136*, 204 – 208.
[107] H. Maune, M. Bockrath, *Appl. Phys. Lett.* **2006**, *89*, 173131-3.
[108] A. Y. Cao, P. L. Dickrell, W. G. Sawyer, M. N. Ghasemi-Nejhad, P. M. Ajayan, *Science* **2005**, *310*, 1307 – 1310.
[109] V. L. Pushparaj, L. J. Ci, S. Sreekala, A. Kumar, S. Kesapragada, D. Gall, O. Nalamasu, A. M. Pulickel, J. Suhr, *Appl. Phys. Lett.* **2007**, *91*, 153116-3.
[110] X. D. Wang, C. J. Summers, Z. L. Wang, *Nano Lett.* **2004**, *4*, 423 – 426.
[111] J. H. Song, X. D. Wang, E. Riedo, Z. L. Wang, *Nano Lett.* **2005**, *5*, 1954 – 1958.
[112] M. H. Zhao, Z. L. Wang, S. X. Mao, *Nano Lett.* **2004**, *4*, 587 – 590.
[113] X. D. Wang, J. H. Song, J. Liu, Z. L. Wang, *Science* **2007**, *316*, 102 – 105.
[114] N. J. Tao, *Nat. Nanotechnol.* **2006**, *1*, 173 – 181.
[115] I. W. P. Chen, M. D. Fu, W. H. Tseng, C. H. Chen, C. M. Chou, T. Y. Luh, *Chem. Commun.* **2007**, 3074 – 3076.
[116] X. Y. Xiao, B. Q. Xu, N. J. Tao, *Angew. Chem.* **2004**, *116*, 6274 – 6278; *Angew. Chem. Int. Ed.* **2004**, *43*, 6148 – 6152.
[117] H. B. Akkerman, P. W. M. Blom, D. M. de Leeuw, B. de Boer, *Nature* **2006**, *441*, 69 – 72.
[118] J. S. Heo, J. H. Chung, J. J. Lee, *Sens. Actuators A* **2006**, *126*, 312 – 327.
[119] Y. Kang, J. J. Walish, T. Gorishnyy, E. L. Thomas, *Nat. Mater.* **2007**, *6*, 957 – 960.
[120] R. R. He, P. D. Yang, *Nat. Nanotechnol.* **2006**, *1*, 42 – 46.
[121] G. Decher, *Science* **1997**, *277*, 1232 – 1237.
[122] V. Maheshwari, R. F. Saraf, *Science* **2006**, *312*, 1501 – 1504.
[123] K. L. Johnson, *Contact Mechanics*, Cambridge University Press, Cambridge, **1985**.
[124] R. F. Saraf, R. S. Porter, *J. Rheol.* **1987**, *31*, 59 – 94.
[125] L. J. Gibson, M. F. Ashby, *Proc. R. Soc. Lond. A* **1982**, *382*, 43 – 59.

